https://doi.org/10.5194/egusphere-2025-2429
Preprint. Discussion started: 5 June 2025

Distribution and cycling of carbon monoxide in surface microlayer and subsurface seawater in the eastern marginal seas of China

Lin Yang [a, b], Peiyi Bian [a], Jing Zhang [b, c, *], Anja Engel [e], Bin Yang [a], Gui-Peng Yang [b, c, d, *]

[a] *Jiangsu Key Laboratory of Marine Bioresources and Environment, Jiangsu Ocean University, Lianyungang, 222005, China*

[b] *Frontiers Science Center for Deep Ocean Multispheres and Earth System, and Key Laboratory of Marine Chemistry Theory and Technology, Ministry of Education, Ocean University of China, Qingdao 266100, China*

[c] *Laboratory for Marine Ecology and Environmental Science, Qingdao National Laboratory for Marine Science and Technology, Qingdao 266237, China*

[d] *Institute of Marine Chemistry, Ocean University of China, Qingdao 266100, China*

[e] *GEOMAR Helmholtz Centre for Ocean Research, 24105 Kiel, Germany*

*Corresponding author:

E-mail address: zhangjouc@ouc.edu.cn (J. Zhang); gpyang@mail.ouc.edu.cn (G.P. Yang)

Keywords: Carbon monoxide; Enrichment Factors; Surface microlayer; Sea-to-air flux; Photoproduction; Bacterial consumption; Eastern marginal seas of China

* Corresponding authors. Key Laboratory of Marine Chemistry Theory and Technology, Ministry of Education, Ocean University of China, Qingdao 266100, China
E-mail addresses: zhangjouc@ouc.edu.cn (J. Zhang); gpyang@mail.ouc.edu.cn (G.P. Yang)

https://doi.org/10.5194/egusphere-2025-2429
Preprint. Discussion started: 5 June 2025

Abstract

Sea-surface microlayer (SML) is the boundary interface between the atmosphere and ocean, exhibiting an enrichment of dissolved organic matter (DOM) and participating in air-sea gas exchange. However, how do DOM enrichment in the SML control the flux of several gases remains poorly understood. In our study, laboratory experiments and in situ investigation in the eastern marginal seas of China were conducted to determine the enrichment factors (EFs) of carbon monoxide (CO) and DOM and their production and consumption rates in the SML during winter. CO, chromophoric DOM (CDOM), and fluorescent DOM (FDOM) were frequently enriched in the SML during winter. Although CO, CDOM and FDOM concentrations decreased from in-shore regions to open ocean, higher EFs of CO and DOM in the SML were generally observed in off-shore regions. Moreover, the EF of CO was lower than EFs of CDOM and FDOM, which appeared to be related to the faster consumption rates of CO in the SML. Considering the photoproduction rate (mean value: 12.4 nmol L^{-1} d^{-1}) was significantly higher than the bacteria consumption rate (mean value: 3.8 nmol L^{-1} d^{-1}) of CO in the SML, the EF and the concentration of CO in SML showed a large diurnal variation, with the higher values observed in the early afternoon. The Flux of CO exhibited a significantly negative correlation with CDOM absorption ($a_{CDOM}(254)$) and fluorescence marine humic-like Component 3 in the SML, suggesting that elevated DOM could stimulate the photoproduction of CO, but may also decrease air-sea CO exchange in the SML.

https://doi.org/10.5194/egusphere-2025-2429
Preprint. Discussion started: 5 June 2025

1. Introduction

Carbon monoxide (CO) plays an important role in atmospheric chemistry (Nguyen et al., 2020). It is the predominant sink of hydroxyl radical (OH•, Conte et al., 2019; Nguyen et al., 2020), which oxidize pollutants and greenhouse gases (such as CH_4) emitted to the atmosphere by human activities (Nguyen., 2020). The photodegradation of dissolved organic matter (DOM) is thought to be the main source of CO in the ocean (Stubbins et al., 2006), and ocean acts as a source of atmospheric CO (Mopper and Kieber, 2002). In addition, direct production of CO by phytoplankton has been observed in laboratory experiments (Gros et al., 2009) and dark/thermal production was also inferred from modeling at Bermuda Atlantic Time Series (BATS, Kettle, 2005), and from incubations of water samples from the Delaware Bay (Xie et al., 2005) and St Lawrence estuary (Zhang et al., 2008). The first time marine production of CO by macroalgae was found by Troxler et al. (1972), which was related to the occurrence of bile pigments. However, direct biological production is still considered to be a minor contributor to the global ocean CO budget (Fichot and Miller, 2010) and dark production has been estimated to account for only 10%–32% of global ocean CO production (Zhang et al., 2006). Microbial consumption and the sea-to-air fluxes (Doney et al., 1995, Song et al., 2015) of CO are considered to be the main sinks of oceanic CO (Zafiriou et al., 2003). CO is rapidly removed from the atmosphere (lifetime of 2 months) by two major processes: geochemical oxidation by atmospheric hydroxyl radicals (85%) and biological oxidation by soil microorganisms (10%) (Cordero et al., 2019). With increasing concern about atmospheric pollution and the

https://doi.org/10.5194/egusphere-2025-2429
Preprint. Discussion started: 5 June 2025

potential role of CO, a primary goal of studying oceanic CO concentrations is to evaluate its long-term stability and distribution trends in the marine boundary layer (Conte et al., 2019; Xu et al., 2023). However, CO has not been widely studied in most coastal regions over the last decade.

The sea surface microlayer (SML) is located at the air-sea interface and is considered to play a critical role in global biogeochemical cycles and climate change by regulating the air-sea exchange of relatively insoluble gases and aerosol particles (Liss and Duce, 1997; Cunliffe et al., 2013). The SML has long been known as a source of gels and airborne particles. For decades, articles have emphasized the presence and enrichment of organic matter in the SML (Liss and Duce, 1997; Orellana et al., 2011). Enrichment Factor (EF) is used to compare the properties of the SML and subsurface water (SSW), and EF of a compound is defined as the ratio of the concentration in the SML to that in the corresponding SSW. Higher EF values of CO and DOM in the SML indicated the significant enrichment properties with respect to SSW waters. In addition, SML is exposed to the most intense solar radiation of any seawater layer, especially ultraviolet (UV) light, and shows significant higher colored dissolved organic matter (CDOM) concentration and microbial abundances compared to the SSW (Obernosterer et al., 2006; Obernosterer et al., 2008; Wurl et al., 2009; Yang et al., 2022), suggesting there are more active photochemical and biochemical processes in the SML. Therefore, SML contains physically, chemically, and biologically distinct environments compared to the SSW (Cunliffe et al., 2011). Surfactants, are amphipathic organic substances that adsorb on aquatic phase boundaries, including the air-sea interface that covers ocean's

https://doi.org/10.5194/egusphere-2025-2429
Preprint. Discussion started: 5 June 2025

surface, and mediate all mass transfer across the SML (Rickard et al., 2019 and 2022). Furthermore, strong spatiotemporal gradients in gas transfer velocity (k_w) were inversely correlated with natural surfactants, especially in the SML and in the underlying near-surface seawater (Pereira et al., 2018). Thus, the present study aimed to clarify the influence of the enrichment of DOM in the SML on sea-air CO exchange by relating seawater DOM concentrations to CO emissions to the atmosphere. CDOM absorption $a_{CDOM}(254)$ is an effective proxy for dissolved organic carbon (DOC) and chlorophyll-*a* (Chl-*a*) concentrations in the eastern marginal seas of China (Yang et al., 2021). It is purported to correspond to absorbance by relatively small, simple compounds (conjugated carbon double bonds) (Lønborg et al., 2018), and it can be used as an indicator for the relatively bio-labile pool of DOM (Guallar and Flos, 2019).

An estimated 10% of surface CO is released into the atmosphere via the sea–to-air interface (Yang et al. 2024). Although intense solar radiation and enrichment of DOM may promote CO photoproduction involving SML (Cunliffe et al., 2013; Pereira et al., 2018; Sugai et al., 2021), and likely modifies sea-to-air gas transfer velocity (*kw*) of CO and other gases (Pereira et al., 2018).The role and response of the SML, along with the complex interplay of biological, geochemical, and physical processes, which govern the transfer of CO from the SSW, where it can either be consumed by bacteria or released into the atmosphere, are much less well understood. Our study hypothesized that SML specific environmental changes (i.e., enrichment processes and biochemical processes) and the abundance and composition of DOM in the eastern marginal seas of China influence the rate of sea-to-air CO exchange, they contribute to the formation of

https://doi.org/10.5194/egusphere-2025-2429
Preprint. Discussion started: 5 June 2025

the marine boundary layer involved in atmospheric chemistry and climate regulation. Our study aimed to clarify the roles of the sea-to-air CO exchange, photochemical production, and biological consumption of CO in SML ($[CO]_{sml}$) and SSW ($[CO]_{sur}$) and establish a CO budget model for the marine boundary layer chemistry.

2. Materials and Methods

2.1 Study Area

The Yellow Sea (YS) and the East China Sea (ECS) are marginal seas of the western Pacific Ocean with complicated hydrological characteristics and are substantially affected by the Yellow Sea Cold Water Mass (YSCWM), the Kuroshio Current, and the coastal currents (Fig. 1). The YSCWM is a low-temperature (< 10°C) and high-salinity (32.0–33.0) water mass. Seawater in the Kuroshio presents high temperatures (20–29°C), high salinities (34.2–34.8), and very low suspended particulate concentrations (SPC) (< 2 mg L^{-1}) (Yang et al., 2022). Changjiang River contributed more than 80% of the total freshwater inflow to the YS and the ECS (Wang et al., 2020). The coastal currents are characterized by low temperatures (9–24 °C), low salinities (15.0–31.5), and high SPC (> 20 mg L^{-1}). There are also considerable freshwater sources draining into the coastal current areas, including the Yalu River, the Changjiang River, and the Min River. Furthermore, the Changjiang River Estuary (CRE) and the adjacent area are greatly affected by diluted water and monsoon, with high nutrients and variable salinity distributions. In addition, the atmospheric circulation in the study area was generally governed by the East Asian

https://doi.org/10.5194/egusphere-2025-2429
Preprint. Discussion started: 5 June 2025

monsoon, with strong northerly winds prevailing from September to April, and low pressure over the northwestern Pacific Ocean producing offshore winds that transported continental air masses into the study area (Li et al., 2019).

2.2 Sampling

We collected 52 paired SML and SSW water samples in the YS and ECS aboard the R/V "*Dong Fang Hong 3*" from 28 December 2019 to 16 January 2020. There were 38 sampling stations during the daytime (7:00-19: 00) and 32 sampling stations during the nighttime (19:00-7: 00). SSW samples were collected at 2–5 m depth using 24 × 10 L Niskin bottles mounted on a rosette equipped with a conductivity–temperature–depth (CTD) profiler. SML sampling used a Garrett Screen (Garrett, 1965) (mesh: 16, wire diameter: 0.36 μm; effective surface area: 2.025 cm^2) according to standard procedures routine in our work (Pereira et al., 2016; Sabbaghzadeh et al., 2017). While SML integrity is disrupted by a moving vessel, or when sampling from its stern (Cunliffe and Wurl, 2014; Wurl et al., 2016), the SML can be successfully sampled from a vessel's bow while on-station (Sabbaghzadeh et al., 2017) with the ambient waterflow toward the RV (Cunliffe and Wurl, 2014). The sampling distance is at a certain distance (5 ~ 8 m) which the CTD sampler was deployed, and CO did not change during the sampling. We therefore adopted this procedure, hand-deploying the Garrett Screen over the bow on the crest of a wave (Cunliffe and Wurl, 2014) and further minimizing potential contamination (engines off, wheelhouse and afterdeck downwind) (Pereira et al., 2016).

The SML samples were collected using the screen sampling technique (Garrett,

https://doi.org/10.5194/egusphere-2025-2429
Preprint. Discussion started: 5 June 2025

1965; Chen et al., 2016; Ma and Yang, 2023) directly off the ship's bow when conditions were calm. Briefly, a screen sampler with a 1.6 mm mesh of stainless-steel wire on a 40 cm × 40 cm stainless steel frame was used. The SML samples were collected in 500 mL brown sample bottles. The screen was held level and dipped into the sea surface, moved laterally to sample from an undisturbed film, and then withdrawn slowly from the surface. Repeated dipping (11 times, 600 mL) was conducted until the desired volume was collected (the depths of the SML samples ranged within 100–500 μm). The screening method is often applied during field studies because of its relative quickness and large sample volume compared to other techniques (Chen et al., 2016). The CO in seawater samples was measured first, immediately after collection. A comparison showed that screen-collected samples usually exhibit greater microlayer enrichment of gas than the plate-collected samples, indicating that the screen sampler might be more effective for in-situ measurements (Yang et al., 2001). CDOM, DOC, and Chl-*a* samples were filtered using 0.7 μm glass fiber filters (GF/F, Whatmann) and the filtrates were transferred to 60- and 40-mL brown glass bottles (pre-cleaned and pre-combusted) for later CDOM and DOC analyses. All samples were frozen (−20 °C) and protected from light. Upon arriving at the land laboratory, samples were analyzed as soon as possible. Sea-surface temperature and salinity were obtained from the sensors on the Seabird 911 CTD rosette. Meteorological data (e.g., wind speed and air temperature) were recorded simultaneously by a ship-borne weather instrument (Li et al., 2019, Table S1). The intensity of incident solar radiation was measured and recorded at half-hour intervals using an OL 756 UV-visible spectroradiometer (Li et al.,

https://doi.org/10.5194/egusphere-2025-2429
Preprint. Discussion started: 5 June 2025

2020, Table S1) fitted with an OL IS-270 2-inch integrating sphere (wavelength accuracy: ± 0.15 nm; wavelength repeatability: ± 0.05 nm; spectral radiance accuracy: 1%). Pearson's product-moment correlation was chosen to identify the relationships between parameters and calculated at the confidence level of 95%.

2.3 Photoexposure experiment

The in-situ natural sunlight incubation experiment was conducted to estimate the CO photoproduction rates in different seawater layers. SSW and SML samples for photochemical incubation were collected from stations B1 and C4, as well as E2, FJ5, P1, and P7, located in the YS and the ECS, respectively. SML and SSW (5 m below seawater surface) samples (SSW: 2 L; SML: 500 mL) were passed through a 0.22 μm PES filters (Pall Corp. Port Washington, NY, USA) immediately to remove the majority of the bacteria and was then placed in an acid-washed and pre-combusted brown glass bottle (2 L) in a natural sunlight incubation. Photo incubation experiments were conducted on the ship immediately after sample collection. To measure the photoproduction at solar radiation production rates of CO, the quartz tubes were treated as follows: (1) uncovered quartz tubes exposed to full-spectrum irradiation; (2) quartz tubes wrapped in multiple layers of aluminum foil to eliminate all light transmission. Treatment (2) was subtracted from light-exposed treatments to remove the fraction of CO produced by dark production. In addition, filtered samples from each site were placed in six 80 mL optically transparent quartz tubes (acid-washed and pre-combusted) and sealed without headspace or air bubbles. The quartz tubes were positioned under

https://doi.org/10.5194/egusphere-2025-2429
Preprint. Discussion started: 5 June 2025

the irradiation source to maximize the exposure of the sample; the water depth in each tube was 5 cm (i.e., the diameter of the tube). Both quartz tubes (SML and SSW) were irradiated for 4 hours and were exposed to direct solar irradiation while being held in a water bath with circulating seawater. The change in the CO photoproduction with time can be seen as a constant due to the relatively small amount of total radiation during the short exposure time. The intensity of incident solar radiation was measured and recorded at half-hour intervals using an OL 756 UV-visible spectroradiometer (Li et al., 2020) fitted with an OL IS-270 2-inch integrating sphere (wavelength accuracy: ± 0.15 nm; wavelength repeatability: ± 0.05 nm; spectral radiance accuracy: 1%, Table S1).

2.4 Microbial Consumption and dark production experiments

Six stations were selected to determine the microbial consumption rates of CO (YS: stations A1, B1 and C4; ECS: stations E2, T2 and S6). CO concentrations of seawater samples were measured immediately upon collection from the SSW and the SML and used as background values. Seawater was used to fill 1 L glass syringes (with a 3-way nylon valve) pre-cleaned with 10% HCl-Milli-Q water and Milli-Q water until headspace-free, and wrapped with Aluminum-foil. The syringes were immersed in a shallow tank of flowing water which were continuously pumped from the sea in order to keep the water temperature of incubation experiments to those of the ambient surface seawater. Each time series of sampling consisted of 4–5 points, and the data from each time series were fitted exponentially to obtain the consumption rate constant (k_{bio}).

Shipboard incubations were conducted to measure CO dark production rates.

https://doi.org/10.5194/egusphere-2025-2429
Preprint. Discussion started: 5 June 2025

According to Zhang et al. (2008), the dark production is the abiotic dark production. Seawater was firstly filtered through 0.45 and 0.2 μm polyethersulfone membranes and bubbled with CO-free gas to reduce the background CO values before being put into the 1 L syringes as previously described. Then syringes were rinsed with the sample water and then overflowed with the sample by 2 times their volumes before they were closed without headspace. All cultures were conducted in duplicate and placed in the same incubator. The water bath was completely darkened with opaque foam and black garbage bags. Samples for measurement were taken from the 1 L syringes every 1–4 h by syringe, taking care to evacuate the headspace after each sampling. The dark production incubations were used to eliminate the effect of dark production from the microbial CO consumption measurements.

2.5 Determination of [CO]

A TA3000R trace gas analyzer (Ametek, USA) was used to measure CO concentrations in the atmosphere and seawater with a lower detection limit of 10 ppbv. Before analysis, the instrument was calibrated using a CO standard gas (nominal concentration: 100 ppbv in zero-grade air; analytical accuracy: ± 2%, State Center for Standard Matter, China). The calibration was repeated every six hours during measurements. The mixing ratio of the CO in the atmosphere was obtained by injecting atmospheric samples from the gas-tight syringe directly into the instrument. The overall uncertainty of the atmospheric CO measurements was estimated to be 8% at a typical mixing ratio of 100 ppbv, including the contributions of instrument accuracy, carrier

https://doi.org/10.5194/egusphere-2025-2429
Preprint. Discussion started: 5 June 2025

gas, and calibration gas. CO in seawater was measured using the headspace equilibrium method (Xie et al., 2002), wherein a 50 ml sample bottle was filled with seawater sample and sealed (as above), and then an equivalent amount of the seawater sample was replaced with 8 mL of high purity nitrogen using a gas-tight syringe. The samples were then shaken at 300 r min^{-1} for 5 min to ensure that the nitrogen-filled headspace in the bottle reached gas-liquid equilibrium before 6 mL of the equilibrated gas was extracted using a gas-tight syringe and injected through a PTFE hydrophobic filter membrane (Millipore, USA) into the TA3000R trace gas analyzer for determination (the PTFE filter membranes were set up to prevent the potential entry of liquid water). The measured equilibrated headspace mixing ratio of CO (ppbv) was corrected using the saturated water vapor pressure and standard atmospheric pressure (Stubbins et al., 2006) and then converted to obtain the concentration of dissolved CO (nmol L^{-1}) in seawater (eq. 4). The method's lower detection limit was 0.02 nmol L^{-1}, with an analytical accuracy of better than 10%.

The daily fluxes (μmol m^{-2} d^{-1}) of CO in the YS and the ECS were calculated using the method reported by Stubbins et al. (2006) and Yang et al. (2011), based on the hourly flux (μmol m^{-2} h^{-1}). These hourly fluxes were examined on the scale of individual days by plotting hourly fluxes against the time of day. Days without full coverage of diurnal variations were discarded, leaving 4 d of data in the final analysis. The area under each daily curve was calculated (OriginPro 8.0) to give daily CO emissions.

The two-layer model proposed by Liss and Merlivat (1986) was used to calculate

https://doi.org/10.5194/egusphere-2025-2429
Preprint. Discussion started: 5 June 2025

the instantaneous sea-to-air flux of CO according to the following equation:

$$F = k([CO]_{surf} - [CO]_{eq}) \quad (1)$$

where F refers to the sea-to-air flux of CO (nmol m^{-2} h^{-1}); and k is the gas transfer coefficient (cm h^{-1}) as a function of wind speed u (m s^{-1}) and the Schmidt number of CO (Sc). In this paper, we used empirical formula E2011 (Edson et al., 2011), which applies to wind speeds from 0 to 18 m s^{-1} (Wind speed ranged from 0.68 m s^{-1} to 12.00 m s^{-1}), to calculate the gas transfer coefficient as follows:

$$k = (0.029u^3 + 5.4)\,(Sc/660)^{-1/2} \quad (2)$$

The Schmidt number of CO was referenced from the research of Zafiriou et al. (2008):

$$Sc = -0.0553t^3 + 4.3825t^2 - 140.07t + 2134 \quad (3)$$

where t is seawater temperature (°C).

$[CO]_{surf}$ represents the initial concentration of CO in the surface seawater, calculated by the following equation:

$$[CO]_{surf} = pm_a\,(\beta pV_w + V_a)/(RTV_w) \quad (4)$$

where *P* is the standard atmosphere pressure (atm) and *ma* represents the concentration of CO in the headspace when the sample reaches equilibrium. β is the Bunsen solubility coefficient which is dependent on salinity and temperature (Wiesenburg and Guinasso, 1979). *Vw* and *Va* are the volumes of seawater and headspace in the sample bottle, respectively. *T* is temperature (in Kelvin) and *R* is the gas constant with the value of 0.08206 atm L $(mol\ K)^{-1}$.

$[CO]_{eq}$ represents the concentration of CO in seawater when atmospheric CO is at

https://doi.org/10.5194/egusphere-2025-2429
Preprint. Discussion started: 5 June 2025

equilibrium with the seawater, calculated by the following equation:

$$[CO]_{eq} = ([CO]_{atm} \times \beta)/M \quad (5)$$

where $[CO]_{atm}$ indicates the mixing ratio of CO in the atmosphere (ppbv); and M is the molar volume of CO under standard pressure and temperature (25.0941 L mol^{-1}). According to the error propagation equation (Nelson et al., 1998), the measurement uncertainty for atmospheric CO can cause an error of 4% in calculating the sea-to-air flux. Most of the error (91%) comes from the uncertainty in the gas transfer coefficient (k).

The turnover time of the photochemical production (τ_{prod}) and biological consumption (τ_{cons}) in the SML was calculated by the following equations (Yang et al., 2005; Yang and Tsunogai, 2005;):

$$\tau_{prod} = [CO] \text{ in SML} \,/\, \text{photochemical CO production rate in SML} \quad (6)$$

$$\tau_{cons} = 1/k_{CO} \text{ in SML} \quad (7)$$

2.6 Determination of CDOM absorption

The Napierian absorption coefficients of CDOM ($a_{CDOM}(\lambda)$ (m^{-1})) were calculated as follows:

$$a_{CDOM}(\lambda) = 2.303\ A_{CDOM}(\lambda)/L \quad (8)$$

where $A_{CDOM}(\lambda)$ is the absorbance of the sample at wavelength λ; and L is the cell pathlength of the quartz cuvette in meters (0.1 m; Stedmon and Markager, 2003). The $a_{CDOM}(254)$ (m^{-1}) was chosen to characterize CDOM abundance.

The spectral slope of the absorption spectrum was obtained by nonlinear fitting of

https://doi.org/10.5194/egusphere-2025-2429
Preprint. Discussion started: 5 June 2025

the absorption coefficient according to the following equation (Stedmon and Markager, 2003):

$$a_{CDOM}(\lambda) = a_{CDOM}(\lambda_0)\exp[-S(\lambda - \lambda_0)] + K \quad (9)$$

where $a_{CDOM}(\lambda)$ and $a_{CDOM}(\lambda_0)$ are the Napierian absorption coefficients at wavelengths λ and λ_0; λ_0 is the reference wavelength; S is the spectral slope of the absorption spectrum; and K represents the background parameters with CDOM removed. The specific UV absorbance ($SUVA_{254}$) can be used to measure aromaticity (Weishaar et al., 2003) and molecular weight (Chowdhury, 2013) of DOM, with higher values generally indicative of higher aromaticity. $SUVA_{254}$ is calculated by dividing the absorbance at 254 nm by DOC. Detailed Chl-*a*, DOC, fluorescence DOM (FDOM), dissolved oxygen (DO), and wavelength (λ)-dependent absorption coefficients of CDOM ($a_{CDOM}(\lambda)$) were determined in the laboratory using published techniques. See supplementary information (Section S1) for analytical details.

2.7 Enrichment factors

The enrichment factor (EF) in the SML is defined as follows:

$$EF = C_M/C_S \quad (10)$$

where C_M is the concentration of any substance in the SML, and C_S is its concentration in the SSW. If the EF of a substance is greater than 1.0, that substance is considered enriched, and if it is less than 1.0, it is considered depleted (Chen et al., 2016). Higher EF mean values of CO and DOM indicated their concentrations were greater in SML than that in the SSW.

https://doi.org/10.5194/egusphere-2025-2429
Preprint. Discussion started: 5 June 2025

2.8 Statistical analyses

The correlation coefficient (r) and probability (P) values were used to evaluate the goodness-of-fit. The correlation matrix, analysis of variance, and principal components analysis were conducted with SPSS version 18.0 (SPSS Inc., Chicago, IL, USA) to test possible relationships between the DOM parameters and environmental factors. P values ≤ 0.05 were considered significant.

3. Results

3.1 Environmental Factors and CO Concentration in the SSW and the SML

Surface water temperature increased from 2.08 °C at YS station H12 to 23.8 °C at ECS station E7 (mean value: 11.85 ± 4.53 °C, Fig. 2). Surface salinity increased from 28.85 at CRE station E1 to 34.62 at ECS station E7 (mean value: 32.35 ± 1.17). Wind speed during sampling ranged from 0.68 m s^{-1} at station H9 to 12.00 m s^{-1} at station FJ1 (mean value: 6.09 ± 2.50 m s^{-1}). In recent years, bubble-mediated enhancement of the transfer velocity, *k*, which exhibits a relationship with wind speed, has emerged as a key issue for flux parameterization in high-wind regions (Edson et al., 2011). The integrated solar irradiance (mean value: 14.09 ± 114.64 kW m^{-2}) during the in-situ incubation ranged from −111.8 kW m^{-2} at YS station H5 to 417.9 kW m^{-2} at ECS station F4.

$a_{CDOM}(254)$ in the YS (SSW: 3.59 ± 0.89 m^{-1}; SML: 4.78 ± 0.85 m^{-1}) was higher than that in the ECS (SSW: 1.64 ± 0.72 m^{-1}; SML: 4.70 ± 3.35 m^{-1}) in both the SML

https://doi.org/10.5194/egusphere-2025-2429
Preprint. Discussion started: 5 June 2025

and the SSW. $a_{CDOM}(254)$ in the SML (4.74 ± 2.50 m^{-1}) showed higher values compared to the SSW (2.52 ± 1.26 m^{-1}) during winter. In addition, no significant difference was observed between $a_{CDOM}(254)$ in the SML and SSW (n = 52, p = 0.76, paired t-test). During the study period, $[CO]_{sur}$ was particularly high at the station F4 (3.61 nmol L^{-1}, sampling time: 12:43) in the SML and relatively high at the station P6 (2.81 nmol L^{-1}, sampling time: 14:36) in the SSW (Fig. 2). The maximum $[CO]_{sml}$ was observed during daytime (sampling time: 12:43, Station F4: 3.61 nmol L^{-1}), but the minimum $[CO]_{sml}$ was observed during night (sampling time: 22:22, Station E2: 0.59 nmol L^{-1}). No significant difference was observed between [CO] in the SML (mean value: 1.54 nmol L^{-1}) and the SSW (mean value: 1.23 nmol L^{-1}) (n = 52, p = 0.11, Wilcoxon signed-rank test). [CO] mean value in the YS (SSW: 1.23 ± 0.40 nmol L^{-1}; SML: 1.54 ± 0.68 nmol L^{-1}) were similar to the concentration observed in the ECS (SSW: 1.23 ± 0.45 nmol L^{-1}; SML: 1.55 ± 0.92 nmol L^{-1}) between the SML and the SSW, respectively. The stronger negative linear relationship observed between salinity and $a_{CDOM}(254)$ was observed in the SSW (r = −0.716, n = 52, p < 0.01) where the influence of terrestrial input in this water layer was higher than that in the SML (r = −0.038, n = 52).

3.2 Variations in parallel factor analysis (PARAFAC)-derived fluorescent DOM components and factors controlling the composition of the fluorescent components

The three fluorescent DOM components were determined statistically by conducting PARAFAC of the samples (Table S1; Fig. S1). Component C1 was apparent with excitation and emission peaks at 275 nm and 335 nm, respectively, and was likely

https://doi.org/10.5194/egusphere-2025-2429
Preprint. Discussion started: 5 June 2025

a tryptophan-like peak T (Yamashita et al., 2017). C2 exhibited excitation/emission (E_x/E_m) maxima at 350 nm/455 nm and similar to peak C derived from terrestrial humic sources (Coble and Paula, 2007). Peak C has often been observed in various coastal (Coble, 1996) and oceanic environments (Yamashita et al., 2017). C3 appeared as a fluorophore with E_x/E_m wavelengths of 320 nm/390 nm and was similar to marine humic-like components from coastal environments (Yamashita and Jaffé, 2008).

3.3 Variation and enrichment of CO, CDOM, DOC, and FDOM in the SML

[CO] showed relatively higher mean value in the SML, where its EFs ranged from 0.34 to 3.6 and it had a mean EF value of 1.3 ± 0.7 (Fig. 3). Up to 92% of CDOM samples were enriched in the SML, with the average EF value of $a_{CDOM}(254)$ of 2.2 ± 1.2, ranging between 0.4 and 6.7. The absorption of CDOM and the fluorescence intensity of FDOM components in the SML were positively correlated with their respective SSW values (Fig. S2), indicating that transport of DOM from the SSW to the SML is an important pathway. The EFs of CO, CDOM, and DOC in the SML were generally higher in the ECS than those in the YS· (Fig. 2 and Fig. S3). The EF of C3, C1 and C2 were 1.6 ± 0.7, 1.4 ± 0.6, and 1.3 ± 0.5, respectively. Furthermore, relatively high CDOM absorption slope mean values ($S_{275\text{-}295}$ and S_R) were observed in the SML (SSW: $S_{275\text{-}295}$: 0.0206 ± 0.0068 and S_R: 1.48 ± 0.49; SML: $S_{275\text{-}295}$: 0.0210 ± 0.0055 and S_R: 1.53 ± 0.22), indicating that CDOM in the SML experienced more significant photodegradation than that in the SSW. The EF of CO in the daytime (mean value: 1.5 ± 0.8, 7:00-19:00) was 1.6 times higher than that in the nighttime (mean value: 0.9 ±

https://doi.org/10.5194/egusphere-2025-2429
Preprint. Discussion started: 5 June 2025

0.3, 19:00-7:00) (Fig. 3b)). The EF of CDOM in the daytime (mean value: 2.3 ± 11.4) was 1.1 times higher than that in the nighttime (mean value: 2.1 ± 0.9) (Fig. 3b)). In addition, $[CO]_{sur}$ in the daytime (mean value: 1.39 ± 0.47 nmol L^{-1}) was 1.3 times higher than that in the nighttime (mean value: 1.05 ± 0.22 nmol L^{-1}) and $[CO]_{sml}$ in the daytime (mean value: 1.88 ± 0.77 nmol L^{-1}) was 2.0 times higher than that in the nighttime (mean value: 0.95 ± 0.29 nmol L^{-1}), likely due to CO photoproduction in the daytime.

3.4 Variation of sea-to-air flux of CO

The atmospheric mixing ratios ($[CO]_{atm}$) of the eastern marginal seas of China ranged from 239 to 900 ppbv with an average of 602 ± 164 ppbv (n = 69; Fig. 2) during winter. $[CO]_{atm}$ measured at the station A1 in the YS (the maximum concentration, sampling time: 5:25) was nearly four times than that measured at the station T2 in the ECS (the minimum concentration, sampling time: 21:12). YS exhibited higher CO mixing ratios (mean value: 423 ppbv in 2007; mean value: 657 ppbv in 2019) than the ECS (mean value: 252 ppbv in 2007; mean value: 476 ppbv in 2019) in this study and a previous study (Yang et al., 2010), indicating $[CO]_{atm}$ showed relatively higher values in the YS than the ECS, and $[CO]_{atm}$ showed a significant decreasing trend from the northern regions to the southern regions in the eastern marginal seas of China (Fig. 2). The higher $[CO]_{atm}$ at the northern stations (the YS) were representative of the regionally polluted continental outflow air mass due to the anthropogenic activity in East Asia.

The instantaneous sea-to-air fluxes of CO ranged from −1.75 to 39.78 nmol m^{-2} h^{-}

https://doi.org/10.5194/egusphere-2025-2429
Preprint. Discussion started: 5 June 2025

^{1} in the SML (4.96 ± 7.35 nmol m^{-2} h^{-1}) and from −0.04 to 34.18 nmol m^{-2} h^{-1} in the SSW (7.40 ± 7.31 nmol m^{-2} h^{-1}). Higher fluxes generally occurred in the southernmost part of the survey area in the ECS (Fig. 2). Although the concentrations of $[CO]_{atm}$ in the northern region were generally higher than those in the southern region, the sea-to-air fluxes of CO in the SML in the ECS (6.94 ± 9.61 nmol m^{-2} h^{-1}) were 3.5 times higher than that in YS (1.97 ± 2.11 nmol m^{-2} h^{-1}), indicated that $[CO]_{atm}$ did not followed the sea-to-air flux of CO shown in Fig. 2. Therefore, $[CO]_{atm}$ values in the YS were heavily depend on land anthropogenic input, but in the ECS, the distribution of $[CO]_{atm}$ were more dependent on the sea-to-air flux of CO.

3.5 CO production and consumption

The photoproduction rate of CO (K_{photo}) under solar irradiance ranged from 0.708 to 1.05 nmol L^{-1} h^{-1} (mean ± SD: 0.860 ± 0.121 nmol L^{-1} h^{-1}) and 0.710 to 1.27 nmol L^{-1} h^{-1} (mean ± SD: 1.03 ± 0.164 nmol L^{-1} h^{-1}) during the in-situ incubation experiments in the SSW and the SML, respectively, as shown in Fig. 4a) and Table 2. The mean value of K_{photo} in the SML was slightly higher than that in the SSW, but the τ_{prod} was lower in the SML (1.35 h) than in the SSW (1.22 h). In addition, a significant relationship was observed between the light-normalized CO production rates between the SML and the SSW ($r = 0.408$, $p < 0.01$, $n = 6$) during winter. The maximum k_{bio} value appeared at the near-shore station B1 and the minimum value at the off-shore station S6 in the SML.

k_{bio} in the SML and the SSW ranged between 1.43 and 3.78 d^{-1} (average ± SD:

https://doi.org/10.5194/egusphere-2025-2429
Preprint. Discussion started: 5 June 2025

2.76 ± 0.80 d^{-1}) and between 1.17 and 3.48 d^{-1} (average ± SD: 2.46 ± 0.88 d^{-1}), respectively, higher than those observed in the Arctic marginal sea (mean ± SD: 0.96 ± 0.29 d^{-1}; Xie et al., 2005), but lower than those in the Northwest Atlantic Ocean (mean ± SD: 6.24 ± 5.76 d^{-1}; Xie et al., 2005) and the China shelf sea (mean ± SD: 4.80 ± 1.82 d^{-1}; Zhang et al., 2019). Thus the bacterial consumption rate constant of CO was low in oligotrophic open ocean regions but higher in productive coastal areas. The turnover times driven by microorganism (τ_{bio}), i.e., the reciprocal of k_{bio}, were 8.9 ± 2.9 h and 11.9 ± 5.4 h in the SML and the SSW, respectively. Since the CO photoproduction rate at the near-shore station B1 was lower than that of the near-shore station E2 and its CO consumption ability was much stronger, the seawater concentration of CO at coastal station E2 (SSW: 1.62 nmol L^{-1}) was higher than that at coastal station B1 (SSW: 1.51 nmol L^{-1}). The microbial consumption rates of CO in the SML varied greatly (average of 0.18 ± 0.05 nmol L^{-1} h^{-1}), higher than the average in the SSW (0.13 ± 0.03 nmol L^{-1} h^{-1}) (Fig. 4b).

3.6 Primary factors controlling the distribution of the optical parameters of DOM and CO and their EFs

Negative relationships were observed between salinity and $a_{CDOM}(254)$ (SSW: $p < 0.01$, $r = -0.715$, $n = 62$; SML: $p = -0.045$, $n = 52$), $a_{CDOM}(355)$ (SSW: $p < 0.01$, $r = -0.622$; SML: $r = -0.146$), and the C1 (SSW: $p < 0.01$, $r = -0.758$, $n = 62$; SML: $r = -0.158$, $n = 52$), C2 (SSW: $p < 0.01$, $r = -0.341$; SML: $r = -0.106$), and C3 (SSW: $p < 0.01$, $r = -0.851$; SML: $r = -0.154$) components in SSW and SML (Table 1). High and

https://doi.org/10.5194/egusphere-2025-2429
Preprint. Discussion started: 5 June 2025

low fluorescence levels of these three components were usually found at sites with low and high salinities, respectively (Fig. 2). These results indicated that riverine inputs mainly determined the distributions of CDOM and FDOM. Furthermore, although significant CO production via CDOM photodegradation has been recorded in estuarine systems (Stubbins et al., 2011), no significant relationships were observed between [CO] and $a_{CDOM}(254)$ in either the SSW or the SML in our study regions. $a_{CDOM}(254)$ ($p < 0.01$, $r = -0.419$, $n = 52$) and the marine humic-like C3 ($p < 0.01$, $r = -0.201$, $n = 52$) were both negatively correlated with the flux of CO in the SML (Fig. 5a and b). The flux of CO was positively related to temperature ($p < 0.01$, $r = 0.511$, $n = 62$) and salinity ($p < 0.01$, $r = 0.338$, $n = 62$) in the SSW (Fig. 5), but the EF of CO showed no significant relationship with surface water temperature, salinity, or mean wind speed during sampling (Fig. 5d and 5f).

4. Discussion

4.1 CO and DOM distribution and enrichment in the SML

The average concentration of $[CO]_{sur}$ (1.23 nmol L^{-1}) in the eastern marginal seas of China was similar to that observed in the Bohai Sea and the YS during autumn (Zhang et al., 2019, 1.22 nmol L^{-1}) and the Arctic waters of the Amundsen Gulf (Beaufort Sea) in September/October (Xie et al., 2009, 0.17–1.34 nmol L^{-1}), but was relatively lower than the Eastern Indian Ocean (Xu et al., 2023, 1.92 nmol L^{-1}). Eastern Indian Ocean, on the other hand, had salinity close to 34 and the temperature was relatively high (around 29°C) in autumn 2020 (Xu et al., 2023). Tropical and subtropical

https://doi.org/10.5194/egusphere-2025-2429
Preprint. Discussion started: 5 June 2025

open ocean regions were generally less affected by terrestrial influences compared to estuarine, coastal and high-latitude areas. CO production and fluxes normalized to discharge is generally higher in warmer waters (Kieber et al., 2014), presumably also partly due to temperature controls on dissolution (Johnson et al., 1996). Therefore, the relatively higher concentration of $[CO]_{sur}$ in in open ocean might be characterized by the relatively high seawater temperature.

$[CO]_{sml}$, $[CO]_{sur}$, DOC and CDOM decreased from coastal regions to open ocean and decreased from the northern sampling area (the YS) to the southern sampling area (the ECS) in both the SSW and the SML (Fig. 2), which was likely due to the input from the land-based sources (Yang et al., 2022). However, CO, CDOM, and FDOM were more frequently enriched in the ECS (Fig. 2). Although CDOM originated from allochthonous terrestrial sources in the ECS and the YS (Yang et al., 2021), CDOM in the ECS was more dominated by photochemical degradation processes, while CDOM in the YS was more influenced by complicated photochemical–biological coupling processes (Zhu et al., 2018). $a_{CDOM}(254)$ and all three fluorescence components were also positively correlated with $SUVA_{254}$ (Table 1), indicating that CDOM showed higher aromaticity and humification in the eastern marginal seas of China. In addition, we observed a significant positive relationship between $a_{CDOM}(254)$ and Chl-*a* in the SSW ($p < 0.01$, $r = 0.333$, $n = 62$), suggesting that phytoplankton biomass and biological processes played an essential role in generating new CDOM and controlling the distribution of CDOM in winter. The EF of marine humic-like Component 3 was significantly higher than the other fluorescence components (1.6 vs. 1.4 and

https://doi.org/10.5194/egusphere-2025-2429
Preprint. Discussion started: 5 June 2025

1.3), indicating that in-situ autochthonous DOM was more strongly enriched in the SML than terrestrial DOM. Thus CO, CDOM, and FDOM were more frequently enriched in the open ocean which were more attributed to the significant local production.

$[CO]_{sur}$ and $[CO]_{sml}$, and the EFs of CO showed strong diurnal fluctuations in our study (Fig. 3, Section 3.1 and 3.3). Similar diurnal fluctuations in $[CO]_{sur}$ have also been observed in other areas (Ren et al., 2010; Yang et al., 2010; Yang et al., 2011), likely resulting from the sunlight-induced photochemical production of CO during daytime and the stronger microbial consumption at night. Significant positive relationships were observed between the EFs of CO and solar irradiance (Table 3). The higher EF values of CO also occurred in the daytime, suggesting that sufficient light and higher temperatures combined to facilitate the photoproduction of CO and its enrichment in the SML.

4.2 Photochemical CO production and biological CO consumption in the SML and the SSW

The mean photoproduction rate of CO in the SML was 1.1 times higher than that in the SSW in the eastern marginal seas of China, and CO in our study region showed a longer turnover time than the findings of Sugai et al. (2021) in Sagami Bay, Japan (τ_{prod} = 0.09 h), which is probably due to relatively low photochemical CO production in the SML and stronger enrichment to long term storage of CO. The dark production rates of CO (k_{dark}) ranged from −0.01 to 4.81 nmol L^{-1} d^{-1}, with a mean value of 1.25 ±

https://doi.org/10.5194/egusphere-2025-2429
Preprint. Discussion started: 5 June 2025

2.34 nmol L^{-1} d^{-1} in the SSW. Zhang et al. (2008) observed that the dark production of CO exhibited a positive linear correlation with the abundance of CDOM, and terrestrial DOM was more efficient at dark producing CO than marine DOM. However, no significant dark production was observed in the SML water samples, which indicated that dark production may be the main factor controlling CO concentrations in deeper seawater.

The turnover times driven by sea-to-air exchange were much longer than those of microbial consumption, about 219 h and 1029 h in the SSW and SML, respectively. This indicated that microbial removal of CO was much faster than sea-to-air exchange, which may make the latter a subordinate pathway for CO removal in our study regions. The relative intense UV light at the surface ocean might influence marine microbial composition and inhibit microbial consumption (Cory and Kling, 2018). However, relatively higher microbial consumption rate of CO in marine systems has been historically attributed to higher Chl-*a*, but lower salinity level (Xie et al., 2009; Yang et al., 2010; Xu et al., 2023). In addition, the heterotrophic bacterial abundance in the SML was ~ 7.5 times greater than in the SSW and the ECS in March 2017 (Sun et al., 2020). The SML is an aggregate-enriched biofilm environment with distinct microbial communities, the diversity of which can differ significantly from underlying waters (Liss and Duce, 2005; Cunliffe et al., 2013). This higher abundance of bacteria could result in the rapid consumption of CO, along with a wide variety of other organic substances in the SML. Thus the CO consumption rate in the SML and the SSW seemed to be, on the whole, less affected by UV radiation. Moreover, elevated nutrient

https://doi.org/10.5194/egusphere-2025-2429
Preprint. Discussion started: 5 June 2025

concentrations can stimulate the growth of phytoplankton, biological activity, and subsequently lead to the abundant production of fresh autochthonous DOM in the SML (Yang et al., 2022). Therefore, compared to the SSW, the elevated DOM concentrations and bacteria abundances could enhance the influences of photoproduction and microbial consumption on CO cycling processes in the SML.

4.3 Implications of CO sea-to-air exchange and emission to the atmosphere

Based on the areas of the ECS (7.7×10^5 km^2) and YS (3.8×10^5 km^2) and their respective CO sea-to-air fluxes, the releases of CO from the ECS and YS to the atmosphere were estimated to range from 3 to 230 Mg CO-C month^{-1} (Mg = 10^6 g) and from –0.2 to 880 Mg CO-C month^{-1}, with averages of 70 Mg CO-C month^{-1} and 10 Mg CO-C month^{-1}, respectively. Clearly, the average annual release of CO to the atmosphere in the ECS was much higher than (nearly 7 times) that in the YS. Yang et al. (2010) suggested that the $[CO]_{sur}$ was the main factor affecting the sea–air flux of CO. However, $[CO]_{sur}$ in the ECS was similar to that in the YS. As noted above, the most likely sources of CO in the SML of these seas are in-situ photoproduction from CDOM and/or vertical export via underlying water. Fig. 2 shows the enhanced higher flux of CO observed in the SML in Changjiang Estuary matched the lowest salinity concentration. Thus the fresh input of the Changjiang River and the mixing processes appear to also promote the sea-to-air CO flux in the SML in the ECS than that in the YS.

Surface-active surfactants are ubiquitous and accumulate in the uppermost < 1000

https://doi.org/10.5194/egusphere-2025-2429
Preprint. Discussion started: 5 June 2025

μm in seawater (Rickard et al., 2019), where they slow the rate of gas exchange between seawater and air (Cunliffe et al., 2013). Rickard et al. (2022) observed that the first-order estimates of the potential suppression of the gas transfer velocity (*kw*) by photo-derived surfactants 12.9%–22.2% in coastal North Sea water. The highest SML enrichments in surfactants have been seen in low productivity, oligotrophic regions away from terrestrial influences, where surfactants concentrations in SSW are generally low (Wurl et al., 2016). Pereira et al. (2018) also noted that the observed reduction in the air-sea CO_2 exchange in the Atlantic Ocean was due to biological surfactants acting as physical barriers and altering turbulent transfer near the water surface. Therefore, the relatively lower fluxes of CO observed in the YS may be indicate seawater contains lots of surfactants in the SML. Despite the clear importance of surfactants at the air-sea interface, we did not conduct surfactant-specific analyses due to the analytical limitations. In our experiments, the CO flux varied by 131% in winter, the negative correlations between $a_{CDOM}(254)$ and the sea-air flux of CO, and between marine humic-like C3 and the sea-air flux of CO suggested that CDOM concentration may reduce the CO sea-air gas exchange rate in our study regions (Fig. 5a and 5b). Therefore, due to the complexity of DOM pool the SML, and its resulting decreased sea-to-air flux of CO, more measurements are needed to validate our conceptual model and provide a better understanding of the flux measurements of CO in the SML.

4.4 Modeling of CO dynamics in the SML and the SSW

All sources and sinks, including photoproduction and dark production, microbial

https://doi.org/10.5194/egusphere-2025-2429
Preprint. Discussion started: 5 June 2025

consumption and sea-air emission, should be considered in estimating CO dynamics in the SML and SSW (Fig. 6). The effective solar illumination period of each day was approximately 12 h, and based on this the average photoproduction rates in the SML and the SSW were calculated to be 12.41 ± 1.87 nmol L^{-1} d^{-1}, 10.32 ± 1.48 nmol L^{-1} d^{-1}, respectively. In the SSW, the ratio of photoproduction to dark production (1.88 ± 2.89 nmol L^{-1} d^{-1}) was about 4:1, and dark production accounted for about 15% of the total production. No dark production of CO was observed in the SML. CO photoproduction was lower in deeper water, while dark production was higher. The calculated contribution of dark production to CO production in this study was similar to that for the St. Lawrence estuary (14%; Zhang and Xie, 2012) but much lower than for the Eastern Indian Ocean (20%; Xu et al., 2023). These were because dark production needs to be given more weight in estimating its contribution to the total production of CO in the deeper waters of the ocean than in estuaries (Xu et al., 2023). The total removal rates of CO were about 2.64 nmol L^{-1} d^{-1} and 2.88 nmol L^{-1} d^{-1} in the SSW and the SML, respectively, including the microbial consumption rates of 2.46 ± 0.88 nmol L^{-1} d^{-1} and 2.76 ± 0.80 nmol L^{-1} d^{-1} in the SSW and the SML, respectively. The sea-to-air exchange rates were 0.18 ± 0.18 nmol L^{-1} d^{-1} in the SSW and 0.12 ± 0.18 nmol L^{-1} d^{-1} in the SML. The turnover of CO occurred faster in the SML environment than in the SSW (~ 1.2 times). Microbial consumption was the primary sink of CO, accounting for about 95% of CO removal, indicating that the biogeochemical cycling of CO is almost entirely contained within seawater and only a small amount of CO is released into the atmosphere (Xie et al., 2005; Yang et al., 2010; Zhang et al., 2019; Xu et al., 2023). The

https://doi.org/10.5194/egusphere-2025-2429
Preprint. Discussion started: 5 June 2025

595 production rates of CO in both SML and SSW significantly exceeds the loss rates, this
596 could lead to accumulation of CO in these systems. Therefore, CO balance in the ECS
597 and YS indicated that the underlying loss of CO (via sea-to-air flux and biodegradation)
598 was slower than the production of CO in the SML, therefore a positive CO balance was
599 maintained in the SML.

600 The average annual photoproduction, microbial consumption, and sea-to-air flux
601 of CO in the SSW were about 3.02, 1.58, and 0.04 Gg CO-C $month^{-1}$, respectively,
602 based on the area of the survey region (~ 1.2×10^6 km^2, SSW ~ 10 m). Conte et al.
603 (2019) used the NEMO-PISCES model combined with original ocean CO data
604 collected worldwide over the last 50 years, ultimately estimating that global emissions
605 of CO to the atmosphere were 4.0 Tg CO-C yr^{-1} (Tg = 10^{12} g). Based on our data, we
606 estimated the contribution of China's eastern marginal seas to global marine CO
607 emissions via sea-to-air flux to be ~ 0.3‰, and the YS and the ECS occupy 2.7‰ of
608 the global ocean area. The simulated surface CO concentrations and sea-to-air fluxes
609 based on our measured values were much smaller than those simulated by Erickson
610 (1989). In our study, CO produced can be rapidly consumed by microorganisms and
611 only a small fraction was released into the atmosphere, which may explain why the
612 relative contribution of the eastern marginal seas of China to atmospheric CO was much
613 lower than the global level.

614 Notably, the enrichment of CO in the SML was more common during the daytime
615 when photochemical processes were more active, but natural sunlight can inhibit the
616 microbial consumption of CO. CO was maximal in the SML, leading to the significant

https://doi.org/10.5194/egusphere-2025-2429
Preprint. Discussion started: 5 June 2025

enrichment and supersaturation. CDOM in the SML experienced more significant photodegradation than that in the SSW as can be seen in Section 3.3. Moreover, researchers assumed that biological, chemical and physical processes in the SML are controlled by changes in DOM concentration at this uppermost thin boundary layer between the ocean and the atmosphere (Cunliffe et al., 2013). We found that autochthonous humic-like DOM was more enriched in the SML than terrestrial DOM, indicating that it could be an indispensable part of CO photoproduction (Yang et al., 2022). Solar irradiance was positively related to the EFs of CO (Table 3), suggesting that the integrated solar irradiance influenced CO enrichment in the SML. Moreover, we did discover the potential for CDOM accumulation in the SML to prevent CO emissions into the atmosphere (Section 4.3). Therefore, CDOM accumulation and the production rates of CO in the SML significantly exceeds the loss rates, this could lead to the significant accumulation of CO in the SML, especially in the daytime.

5. Conclusions

The present study represents the first comprehensive investigation of CO distribution, loss, and production processes in both the SML and SSW, as well as sea-to-air CO flux in the ECS and YS during winter. $[CO]_{sur}$, $[CO]_{sml}$, CDOM, FDOM, and DOC were generally decreased from coastal regions toward open ocean. However, the EFs of CO, CDOM, FDOM, and DOC were significantly higher in offshore regions, suggesting that stronger enrichment processes in the SML are more prevalent in open waters compared to coastal areas. CDOM absorption slope mean values ($S_{275\text{-}295}$ and S_R) demonstrated that CDOM in the SML underwent more substantial

https://doi.org/10.5194/egusphere-2025-2429
Preprint. Discussion started: 5 June 2025

photodegradation than that in the SSW. Notably, the EF of the marine humic-like C3 was significantly higher than other fluorescence components, indicating that in-situ autochthonous DOM was more strongly enriched in the SML than terrestrial DOM. Significant negative correlations were observed between $a_{CDOM}(254)$ and sea-to-air CO flux, as well as between sea-to-air CO flux and humic-like C3 in the SML, indicating that the open sea exhibit lower CDOM concentrations but higher gas transfer suppression of CO compared to nearshore waters, and that the enrichment of in-situ autochthonous DOM may regulate CO emissions to the atmosphere in the SML. The observed diurnal variability in CO EF led us to conclude that in-situ photoproduction processes play a crucial role in determining CO distribution within the SML. Our findings reveal a complex interplay between DOM enrichment and sea-air CO fluxes in the SML, the connection that should be incorporated into future budget models for accurate carbon cycling assessments in marine environments.

Author contribution

Lin Yang: Conceptualization, Writing-Original Draft, Writing-Review and Editing

Peiyi Bian: Formal analysis

Jing Zhang: Writing-Review and Editing, Funding acquisition

Anja Engel: Writing-Review and Editing

Bin Yang: Writing-Review and Editing

Gui-Peng Yang: Writing-Review and Editing, Supervision

https://doi.org/10.5194/egusphere-2025-2429
Preprint. Discussion started: 5 June 2025

Competing interests

The authors declare that they have no known competing financial interests or personal relationships that could have appeared to influence the work reported in this paper.

Acknowledgment

We are grateful to the captain and crew of the R/V "*Dong Fang Hong 3*" for their help and cooperation during the in-situ investigation. This study was financially supported by the National Natural Science Foundation of China (Grant No. 42330402), and the National Key Research and Development Program (Grant No. 2016YFA0601300).

https://doi.org/10.5194/egusphere-2025-2429
Preprint. Discussion started: 5 June 2025

References

Chen, Y., Yang, G., Xia, Q., Wu, G., 2016. Enrichment and characterization of dissolved organic matter in the surface microlayer and subsurface water of the South Yellow Sea. Mar. Chem. 182(Mar. 20), 1–13. doi: 10.1016/j.marchem.2016.04.001

Chowdhury, S., 2013. Trihalomethanes in drinking water: effect of natural organic matter distribution. WATER SA, 39, 1–7. doi: 10.4314/wsa.v39i1.1

Coble, P.G., 1996. Characterization of marine and terrestrial DOM in seawater using excitation-emission matrix spectroscopy. 51(4), 325–346. doi: 10.1016/0304-4203(95)00062-3

Coble, P.G., Paula, G., 2007. Marine optical biogeochemistry: the chemistry of ocean color. Cheminform 38(2), 402–418. doi: 10.1002/chin.200720265

Conte, L., Szopa, S., Séférian, R., Bopp, L., 2019. The oceanic cycle of carbon monoxide and its emissions to the atmosphere. Biogeosciences, 16(4), 881–902. doi: 10.5194/bg-16-881-2019

Cordero, P.R.F., Bayly, K., Leung, P.M., Huang, C., Greening, C., 2019. Atmospheric carbon monoxide oxidation is a widespread mechanism supporting microbial survival. ISME J. 13(14). doi: 10.1038/s41396-019-0479-8

Cory, R.M., Kling, G.W., 2018. Interactions between sunlight and microorganisms influence dissolved organic matter degradation along the aquatic continuum. Limnol. Oceanogr. Lett. 3(3), 102–116. doi: 10.1002/lol2.10060

Cunliffe, M., Engel, A., Frka, S., Gašparovi, B., Guitart, C., Murrell, J.C., Salter, M., Stolle, C., Upstill-Goddard, R., Wurl, O., 2013. Sea surface microlayers: A unified physicochemical and biological perspective of the air-ocean interface. Prog. Oceanogr. 109, 104–116. doi: 10.1016/j.pocean.2012.08.004

https://doi.org/10.5194/egusphere-2025-2429
Preprint. Discussion started: 5 June 2025

694 Cunliffe, M., Upstill-Goddard, R.C., Murrell, J.C., 2011. Microbiology of aquatic
695 surface microlayers. FEMS Microbiol. Rev. 35(2), 233–246. doi:
696 10.1111/j.1574 - 6976.2010.00246.x
697 Cunliffe, M., Wurl, O., 2014. Guide to best practices to study the ocean's surface.
698 Occasional Publications of the Marine Biological Association of the United
699 Kingdom, Plymouth, UK. 118 pp.
700 Doney, S.C., Najjar, R.G., Stewart, S., 1995. Photochemistry, mixing and diurnal cycles
701 in the upper ocean. J. Mar. Res. 53(3), 341–369. doi: 10.1357/0022240953213133
702 Edson, J.B., Fairall, C.W., Bariteau, L., Zappa, C.J., Cifuentes-Lorenzen, A., Mcgillis,
703 W.R., Pezoa, S., Hare, J.E., Helmig, D., 2011. Direct covariance measurement of
704 CO_2 gas transfer velocity during the 2008 Southern Ocean Gas Exchange
705 Experiment: Wind speed dependency. J. Geophys. Res. 116(C4), 1943–1943. doi:
706 10.1029/2011jc007022
707 Engel, A., Galgani, L., 2016. The organic sea-surface microlayer in the upwelling
708 region off the coast of Peru and potential implications for air–sea exchange
709 processes. Biogeosciences 13, 989–1007. doi: 10.5194/bg-13-989-2016
710 Erickson, D.J., 1989. Ocean to atmosphere carbon monoxide flux: Global inventory
711 and climate implications. Global Biogeochem. Cyc. 3(4), 305–314. doi:
712 10.1029/GB003i004p00305
713 Fichot, C.G., Miller, W.L., 2010. An approach to quantify depth-resolved marine
714 photochemical fluxes using remote sensing: application to carbon monoxide (CO)
715 photoproduction. Remote Sens. Environ. 114, 1363–1377. doi:
716 10.1016/j.rse.2010.01.019
717 Garrett, W.D., 1965. Collection of slick-forming materials from the sea surface. Limnol.

https://doi.org/10.5194/egusphere-2025-2429
Preprint. Discussion started: 5 June 2025

718 Oceanogr. 10(1965), 602–605. doi: 10.2307/2833459

719 Gros, V., Peeken, I., Bluhm, K., Zöllner, E., Sarda-Esteve, R., Bonsang, B., 2009.
720 Carbon monoxide emissions by phytoplankton: evidence from laboratory
721 experiments. Environ. Chem. 6, 369–379. doi: 10.1071/EN09020

722 Guallar, C., Flos, J., 2019. Linking phytoplankton primary production and
723 chromophoric dissolved organic matter in the sea. Prog. Oceanogr. 176, 102116.
724 doi: 10.1016/j.pocean.2019.05.008

725 Johnson, J.E., Bates, T.S., 1996. Sources and sinks of carbon monoxide in the mixed
726 layer of the tropical south Pacific Ocean. Global Biogeochem. Cy. 10(2), 347–359.
727 doi: 10.1029/96GB00366

728 Kettle, A.J., 2005. Diurnal cycling of carbon monoxide (CO) in the upper ocean near
729 Bermuda. Ocean Model. 8(4), 337–367. doi: 10.1016/j.ocemod.2004.01.003

730 Kieber, D.J., Miller, G.W., Neale, P.J., Mopper, K., 2014. Wavelength and temperature-
731 dependent apparent quantum yields for photochemical formation of hydrogen
732 peroxide in seawater. Env. Sci.: Processes Impacts. doi: 10.1039/C4EM00036F.

733 Li, Y., He, Z., Yang, G.P., Wang, H., Zhuang, G.C., 2019. Volatile halocarbons in the
734 marine atmosphere and surface seawater: diurnal and spatial variations and
735 influences of environmental factors. Atmos. Environ. 214, 116820.
736 10.1016/j.atmosenv.2019.116820

737 Li, Y., Fichot, C.G., Geng, L., Scarratt, M.G., Xie, H., 2020. The Contribution of
738 Methane Photoproduction to the Oceanic Methane Paradox. Geophys. Res. Lett.
739 47(14), 1–10. doi: 10.1029/2020GL088362

740 Liss, P.S., Merlivat, L., 1986. Air-sea gas exchange rates: Introduction and synthesis.

https://doi.org/10.5194/egusphere-2025-2429
Preprint. Discussion started: 5 June 2025

In P. Buat-Ménard (Ed.), The role of air-sea exchange in geochemical cycling, (pp. 113–127). Dordrecht, Netherlands: Springer. Retrieved from papers3://publication/uuid/BAFDE7E6-A29C-466C-B1CD-2A7DAFF930D5

Liss, P.S., Duce, R.A., (Eds) 1997. The sea surface and global change. Cambridge, UK: Cambridge University Press.

Liss, P.S., Duce, R.A., 2005. The Sea Surface and Global Change, Cambridge University Press, UK, ISBN-13: 978-0511525025.

Lønborg, C., Álvarez-Salgado, X.A., Duggan, S., Carreira, C., 2018. Organic matter bioavailability in tropical coastal waters: The Great Barrier Reef. Limnol. Oceanogr. 63, 1015–1035. doi: 10.1002/lno.10717

Ma, Q.Y., Yang, G.P., 2023. Roles of phytoplankton, microzooplankton, and bacteria in DMSP and DMS transformation processes in the East China Continental Sea. Prog. Oceanogr. 103003. doi: 10.1016/j.pocean.2023.103003

Mopper, K., Kieber, D.J., 2002. Photochemistry and cycling of carbon, sulfur, nitrogen and phosphorus. In: Hansell, D.A., Carlson, C.A. (Eds.), Biogeochemistry of Marine Dissolved Organic Matter. AP. doi: 10.1016/b978-012323841-2/50011-7

Nelson, E.D., McConnell, L.L., Baker, J.E., 1998. Diffusive Exchange of Gaseous Polycyclic Aromatic Hydrocarbons and Polychlorinated Biphenyls Across the Air−Water Interface of the Chesapeake Bay. Environ. Sci. Technol. 32(7), 912–919. doi: 10.1021/es9706155

https://doi.org/10.5194/egusphere-2025-2429
Preprint. Discussion started: 5 June 2025

761 Nguyen, N.H., Turner, A.J., Yin, Y., Prather, M.J., Frankenberg, C., 2020. Effects of
762 chemical feedbacks on decadal methane emissions estimates. Geophys. Res. Lett.
763 47(3), e2019GL085706. doi: 10.1029/2019GL085706
764 Obernosterer, I., Catala, P., Reinthaler, T., Herndl, G.J., Lebaron, P., 2006. Enhanced
765 heterotrophic activity in the surface microlayer of the Mediterranean Sea. Aquat.
766 Microb. Ecol. 39, 293–302. doi: 10.3354/ame039293
767 Obernosterer, I., Catala, P., Lami, R., Caparros, J., Ras, J., Bricaud, A., Dupuy, C., van
768 Wambeke, F., Lebaron, P., 2008. Biochemical characteristics and bacterial
769 community structure of the sea surface microlayer in the South Pacific Ocean.
770 Biogeosciences, 5, 693–705. doi: 10.5194/bg-5-693-2008
771 Orellana, M.V., Matrai, P.A., Leck, C., Rauschenberg, C.D., Lee, A.M., Coz, E., 2011.
772 Marine microgels as a source of cloud condensation nuclei in the high Arctic. Proc.
773 Natl. Acad. Sci. 108, 13612–13617. doi: 10.1073/pnas.1102457108.
774 Pereira, R., Schneider-Zapp, K., Upstill-Goddard, R.C., 2016. Surfactant control of gas
775 transfer velocity along an offshore coastal transect: results from a laboratory gas
776 exchange tank. Biogeosciences, 13, 3981–3989. doi: 10.5194/bg-13-3981-2016.
777 Pereira, R., Ashton, I., Sabbaghzadeh, B., Shutler, J.D., Upstill-Goddard, R.C., 2018.
778 Reduced air–sea CO_2 exchange in the Atlantic Ocean due to biological surfactants.
779 Nat. Geosci. 11, 492–496. doi: 10.1038/s41561-018-0136-2
780 Ren, C., Yang, G., Lu, X., 2014. Autumn photoproduction of carbon monoxide in
781 Jiaozhou Bay China. J. Ocean U. China, 13(3), 428–436. doi: 10.1007/s11802-
782 014-2225-1

https://doi.org/10.5194/egusphere-2025-2429
Preprint. Discussion started: 5 June 2025

Rickard, P.C., Uher, G., Upstill-Goddard, R.C., Frka, S., Mustaffa, N.I.H., Banko-Kubis, H.M., Hanne Marie, B.K., Ana Cvitesic, K., Blazenka, G., Christian, S., Oliver, W., 2019. Reconsideration of seawater surfactant activity analysis based on an inter-laboratory comparison study. Mar. Chem. 208, 103–111. doi: 10.1016/j.marchem.2018.11.012

Rickard, P.C., Uher, G., Upstill-Goddard, R.C., 2022. Photo-reactivity of surfactants in the sea-surface microlayer and subsurface water of the Tyne estuary, UK. Geophys. Res. Lett. 49(4), e2021GL095469. doi: 10.1029/2021GL095469

Sabbaghzadeh, B., Upstill-Goddard, R.C., Beale, R., Pereira, R., Nightingale, P.D., 2017. The Atlantic Ocean surface microlayer from 50°N to 50°S is ubiquitously enriched in surfactants at wind speeds up to 13 m s^{-1}. Geophys. Res. Lett. 44(6), 2852–2858. doi: 10.1002/2017GL072988

Song, G., Richardson, J.D., Werner, J.P., Xie, H., Kieber, D.J., 2015. Carbon monoxide photoproduction from particles and solutes in the Delaware estuary under contrasting hydrological conditions. Environ. Sci. Technol. 49(24), 14048–14056. doi: 10.1021/acs.est.5b02630

Stedmon, C.A., Markager, S., Bro, R., 2003. Tracing dissolved organic matter in aquatic environments using a new approach to fluorescence spectroscopy. Mar. Chem. 82(3–4), 239–254. doi: 10.1016/S0304-4203(03)00072-0

Stubbins, A., Uher, G., Kitidis, V., Law, C.S., Upstill-Goddard, R.C., Woodward, E.M.S., 2006. The open-ocean source of atmospheric carbon monoxide. Deep-Sea Res. Part II, 53, 1685–1694. doi: 10.1016/j.dsr2.2006.05.010

Stubbins, A., Law, C., Uher, G., Upstill-Goddard, R., 2011. Carbon monoxide apparent quantum yields and photoproduction in the Tyne estuary. Biogeosciences 8, 703–713. doi:10.5194/bg-8-703-2011

https://doi.org/10.5194/egusphere-2025-2429
Preprint. Discussion started: 5 June 2025

Sugai, Y., Tsuchiya, K., Shimode, S., Toda, T., 2021. Photochemical Production and Biological Consumption of CO in the SML of Temperate Coastal Waters and Their Implications for Air-Sea CO Exchange. J. Geophys. Res.: Oceans 125(4), 1–14. doi: 10.1029/2019JC015505

Sun, H., Zhang, Y.H., Tan, S., Zheng, Y.F., Zhou, S., Ma, Q.Y., Yang, G.P., Todd, J., Zhang, X.H., 2020. DMSP-Producing Bacteria Are More Abundant in the Surface Microlayer than Subsurface Seawater of the East China Sea. Microb. Ecol. 80, 350–365. doi: 10.1007/s00248-020-01507-8

Troxler, R.F., 1972. Synthesis of bile pigments in plants. Formation of carbon monoxide and phycocyanobilin in wild-type and mutant strains of the alga, Cyanidium caldarium. Biochemistry 11(23), 4235–4242. doi: 10.1021/bi00773a007

Tsai, W.T., Liu, K.K., 2003. An assessment of the effect of sea surface surfactant on global atmosphere–ocean CO_2 flux. J. Geophys. Res.: Oceans 108, 3127. doi: 10.1029/2000jc000740

Wang, H., Sun, F., Liu, W., 2020. Characteristics of Streamflow in the Main stream of Changjiang River and the Impact of the Three Gorges Dam. Catena 104498. doi: 10.1016/j.catena.2020.104498

Weishaar, J.L., Aiken, G.R., Bergamaschi, B.A., Fram, M.S., Fujii, R., Mopper, K., 2003. Evaluation of specific ultraviolet absorbance as an indicator of the chemical composition and reactivity of dissolved organic carbon. Environ. Sci. Technol. 37, 4702–4708. doi: 10.1021/es030360x

Wiesenburg, D.A, Guinasso, N.L., 1979. Equilibrium solubilities of methane, carbon monoxide, and hydrogen in water and sea water. J. Chem. Eng. Data, 24(4), 356–360. doi: 10.1021/je60083a006

https://doi.org/10.5194/egusphere-2025-2429
Preprint. Discussion started: 5 June 2025

832 Wurl, O., Miller, L., Röttgers, R., Vagle, S., 2009. The distribution and fate of surface-
833 active substances in the sea-surface microlayer and water column. Mar. Chem. 115,
834 1–9. doi: 10.1016/j.marchem.2009.04.007
835 Wurl, O., Stolle, C., Thuoc, C.V., Thu, P.T., Mari, X., 2016. Biofilm-like properties of
836 the sea surface and predicted effects on air-sea CO_2 exchange. Prog. Oceanogr.
837 144, 15–24. doi: 10.1016/j.pocean.2016.03.002
838 Xie, H., Andrews, S.S., Martin, W.R., Miller, J., Zafiriou, O.C., 2002. Validated
839 methods for sampling and headspace analysis of carbon monoxide in seawater.
840 Mar. Chem. 77(2), 93–108. doi: 10.1016/S0304-4203(01)00065-2
841 Xie, H., Zafiriou, O.C., Umile, T.P., Kieber, D.J., 2005. Biological consumption of
842 carbon monoxide in Delaware Bay, NW Atlantic and Beaufort Sea. Mar. Ecol.
843 Prog. Seri. 290, 1–14. doi: 10.3354/meps290001
844 Xie, H.X., Bélanger, S., 2009. Photobiogeochemical cycling of carbon monoxide in the
845 southeastern Beaufort Sea in spring and autumn. Limnol. Oceanogr. 54(1), 234–
846 249. doi: 10.4319/lo.2009.54.1.0234
847 Xu, G.B., Xu, F., Ji, X., Zhang, J., Yan., S.B., Mao, S.H., Yang, G.P., 2023. Carbon
848 monoxide cycling in the Eastern Indian Ocean. J. Geophys. Res. Oceans 128(5).
849 doi: 10.1029/2022JC019411
850 Yamashita, Y., Hashihama, F., Saito, H., Fukuda, H., Ogawa, H., 2017. Factors
851 controlling the geographical distribution of fluorescent dissolved organic matter
852 in the surface waters of the Pacific Ocean. Limnol. Oceanogr. 62(6), 2360–2374.
853 doi: 10.1002/lno.10570
854 Yamashita, Y., Jaffé, R., 2008. Characterizing the interactions between trace metals and
855 dissolved organic matter using excitation-emission matrix and parallel factor

https://doi.org/10.5194/egusphere-2025-2429
Preprint. Discussion started: 5 June 2025

analysis. Environ. Sci. Technol. 42(19), 7374–7379. doi: 10.1021/es801357h

Yang, G.P., Ren, C.Y., Lu, X.L., Liu, C.Y., Ding, H.B., 2011. Distribution, flux, and photoproduction of carbon monoxide in the East China Sea and Yellow Sea in spring. J. Geophys. Res.: Oceans 116(C2), C02001. doi: 10.1029/2010jc006300

Yang, G.P., Wang, W.L., Lu, X.L., Ren, C.Y., 2010. Distribution, flux and biological consumption of carbon monoxide in the Southern Yellow Sea and the East China Sea. Mar. Chem. 122(1–4), 74–82. doi: 10.1016/j.marchem.2010.08.001

Yang, L., Zhang, J., Yang, G.P., 2021. Mixing behavior, biological and photolytic degradation of dissolved organic matter in the East China Sea and the Yellow Sea. Sci. Total Environ. 762(6), 143164. doi: 10.1016/j.scitotenv.2020.143164

Yang, L., Zhang, J., Engel A., Yang, G.P., 2022. Spatio-temporal distribution, photoreactivity and environmental control of dissolved organic matter in the sea-surface microlayer of the eastern marginal seas of China. Biogeosciences, 19, 5251–5268. doi: 10.5194/bg-19-5251-2022

Yang, L., Gong, C.Y., Mo, X.J., Zhang, J., Yang, B., Yang, G.P., 2024. Carbon monoxide in the marine atmosphere and seawater: Spatiotemporal distribution and photobiogeochemical cycling. J. Geophys. Res.: Oceans, 129(8), e2024JC021286. doi: 10.1029/2024JC021286

Zafiriou, O.C., Andrews, S.S., Wang W., 2003. Concordant estimates of oceanic carbon monoxide source and sink processes in the Pacific yield a balanced global "blue-water" CO budget. Global Biogeochem. Cy. 17(1), 1015–1027. doi: 10.1029/2001gb001638

Zafiriou, O.C., Xie, H., Nelson, N.B., Wang, N.W., 2008. Diel carbon monoxide cycling in the upper Sargasso Sea near Bermuda at the onset of spring and in midsummer. Limnol. Oceanogr. 53(2), 835–850. doi: 10.2307/40006463

https://doi.org/10.5194/egusphere-2025-2429
Preprint. Discussion started: 5 June 2025

881 Zhang, J., Wang, J., Zhuang, G.C., Yang G.P., 2019. Carbon monoxide cycle in the
882 Bohai Sea and the Yellow Sea: Spatial variability, sea-air exchange and biological
883 consumption in autumn. J. Geophys. Res.: Oceans 124, 4248–4257. doi:
884 10.1029/2018JC014864
885 Zhang, Y., Xie, H., 2012. The sources and sinks of carbon monoxide in the St. Lawrence
886 system. Deep-Sea Res. Part II: Topical Studies in Oceanography 81, 114–123. doi:
887 10.1016/j.dsr2.2011.09.003
888 Zhang, Y., Xie, H., Chen, G., 2006. Factors affecting the efficiency of carbon monoxide
889 photoproduction in the St. Lawrence estuarine system (Canada). Environ. Sci.
890 Technol. 40(24), 7771–7777. doi: 10.1021/es0615268
891 Zhang, Y., Xie, H., Fichot, C.G., Chen, G., 2008. Dark production of carbon monoxide
892 (CO) from dissolved organic matter in the St. Lawrence estuarine system:
893 Implication for the global coastal and blue water CO budgets. J. Geophys. Res.:
894 Oceans 113(12), 1–9. doi: 10.1029/2008JC004811
895 Zhu, W.Z., Zhang, H.H., Zhang, J., Yang, G.P., 2018. Seasonal variation in
896 chromophoric dissolved organic matter and relationships among fluorescent
897 components, absorption coefficients, and dissolved organic carbon in the Bohai
898 Sea, the Yellow Sea and the East China Sea. J. Mar. Syst. 180, 9–23. doi:
899 10.1016/j.jmarsys.2017.12.003
900

https://doi.org/10.5194/egusphere-2025-2429
Preprint. Discussion started: 5 June 2025

901

902 **Figure Captions**

903 **Fig. 1.** Map of sampling stations in the East China Sea and the Yellow Sea during winter. Red box
904 represented photochemical incubation experiment stations and purple rhomboid represented
905 biological consumption experiment stations

906 ■: Stations for CO microbial consumption incubation experiments; ▲: Stations for CO
907 photochemical production incubation experiments; ★: Station for both CO microbial consumption
908 and photochemical production incubation experiments; ●: Stations only for seawater sampling.

909 **Fig. 2.** Distributions of CO and the marine-like fluorescence C3 in the SSW and the SML; CO in
910 the atmosphere, and the flux of CO in the SSW and the SML; and the enrichment factors of CO and
911 the marine-like fluorescence C3 in the SML, and temperature and salinity in the in the East China
912 Sea and the Yellow Sea during winter. The concentration profiles of CO in the SSW (d) resemble
913 those of CO in the SML, which is evidence for biogeochemically very stable, salt-like (conservative)
914 properties.

915 **Fig. 3.** Variations in the $[CO]_{sml}$, $[CO]_{ssw}$, $a_{CDOM}(254)$, and DOC, EFs of [CO], $a_{CDOM}(254)$, and
916 DOC with the sampling time at each station.

917 **Fig. 4.** Variations in photochemical CO production rate of CO (K_{photo}) in the SML (red) and the
918 SSW (black) (a)). Variations in microbial consumption rate constants of CO (K_{bio}) in the SML (red)
919 and the SSW (black).

920 **Fig. 5.** Correlations between the instantaneous sea-to-air fluxes of CO (Flux) in the SSW and the
921 SML with $a_{CDOM}(254)$, marine humic-like C3, wind speeds, temperature, and salinity in the East
922 China Sea and the Yellow Sea during winter.

https://doi.org/10.5194/egusphere-2025-2429
Preprint. Discussion started: 5 June 2025

Fig. 6. Budget model of CO transformation in the SML and the SSW in the eastern marginal seas of China during winter. (The arrows represent simplified processes of CO, CDOM and bacteria in the SML and the SSW. Solid arrows represent CO sources (red) or sinks (blue) processes, and CO, CDOM, bacteria enrichment (black) processes. The production (red) and removal (blue) rates and their individual contributions percentages represent simplified transformation processes of CO in the SML and the SSW. The black percentage represent the enrichment processes of CO, CDOM and bacteria in the SML. Bacterial enrichment was calculated by Sun et al., 2020).

https://doi.org/10.5194/egusphere-2025-2429
Preprint. Discussion started: 5 June 2025

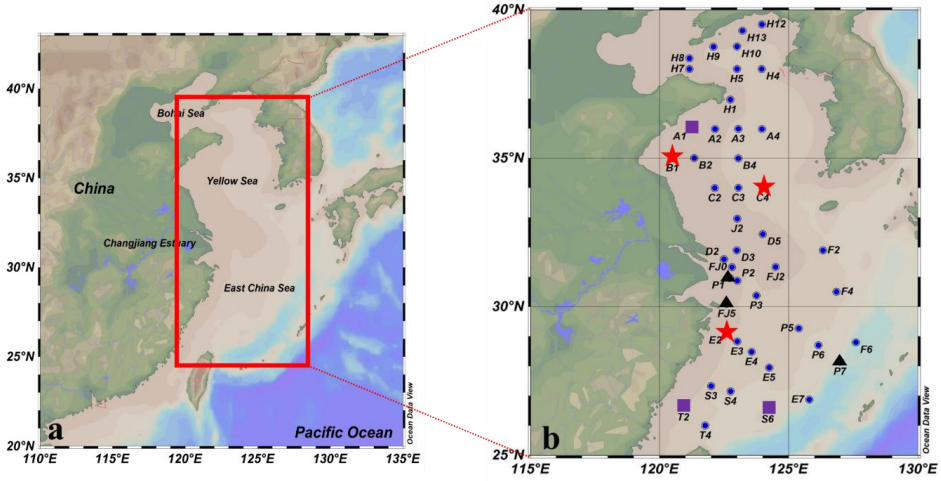

Fig. 1. Map of sampling stations in the East China Sea and the Yellow Sea during winter. Red box represented photochemical incubation experiment stations and purple rhomboid represented biological consumption experiment stations.

■: Stations for CO microbial consumption incubation experiments; ▲: Stations for CO photochemical production incubation experiments; ★: Station for both CO microbial consumption and photochemical production incubation experiments; ●: Stations only for seawater sampling.

https://doi.org/10.5194/egusphere-2025-2429
Preprint. Discussion started: 5 June 2025

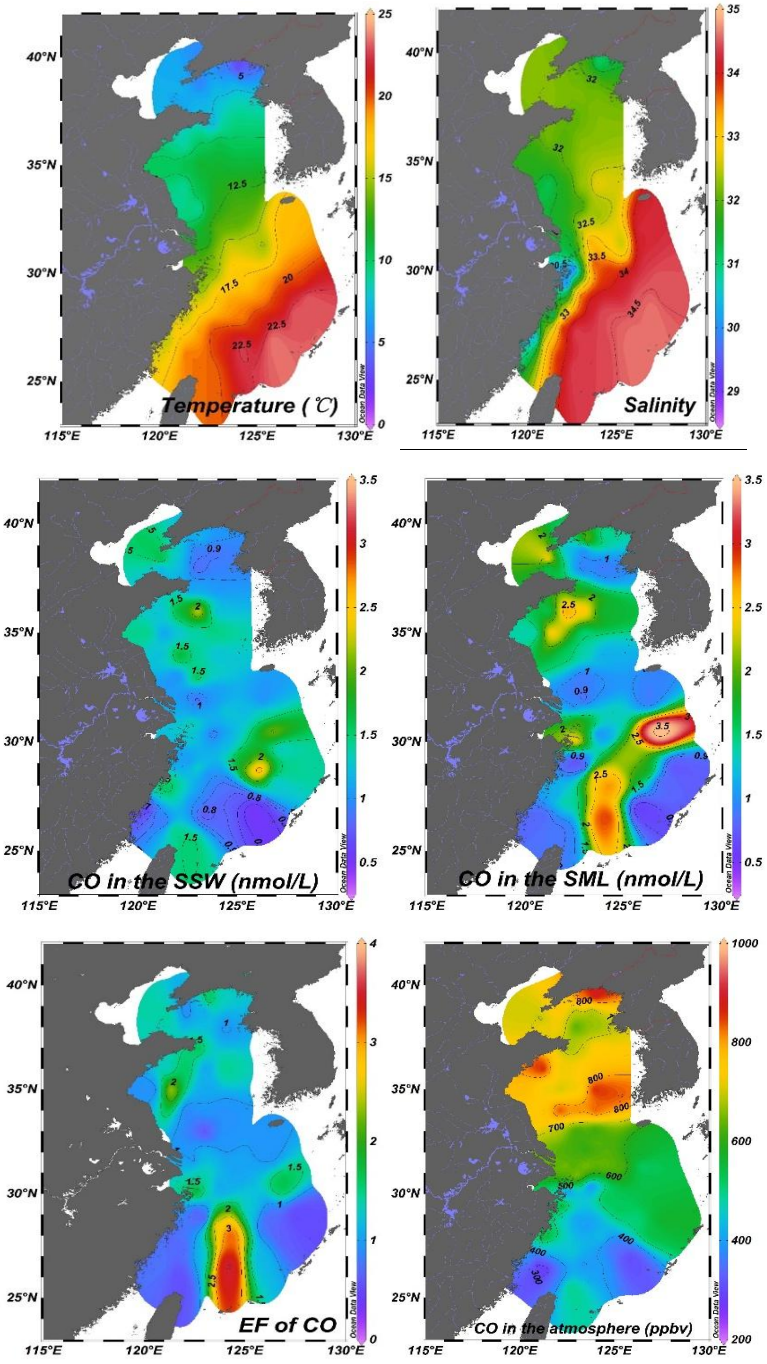

https://doi.org/10.5194/egusphere-2025-2429
Preprint. Discussion started: 5 June 2025

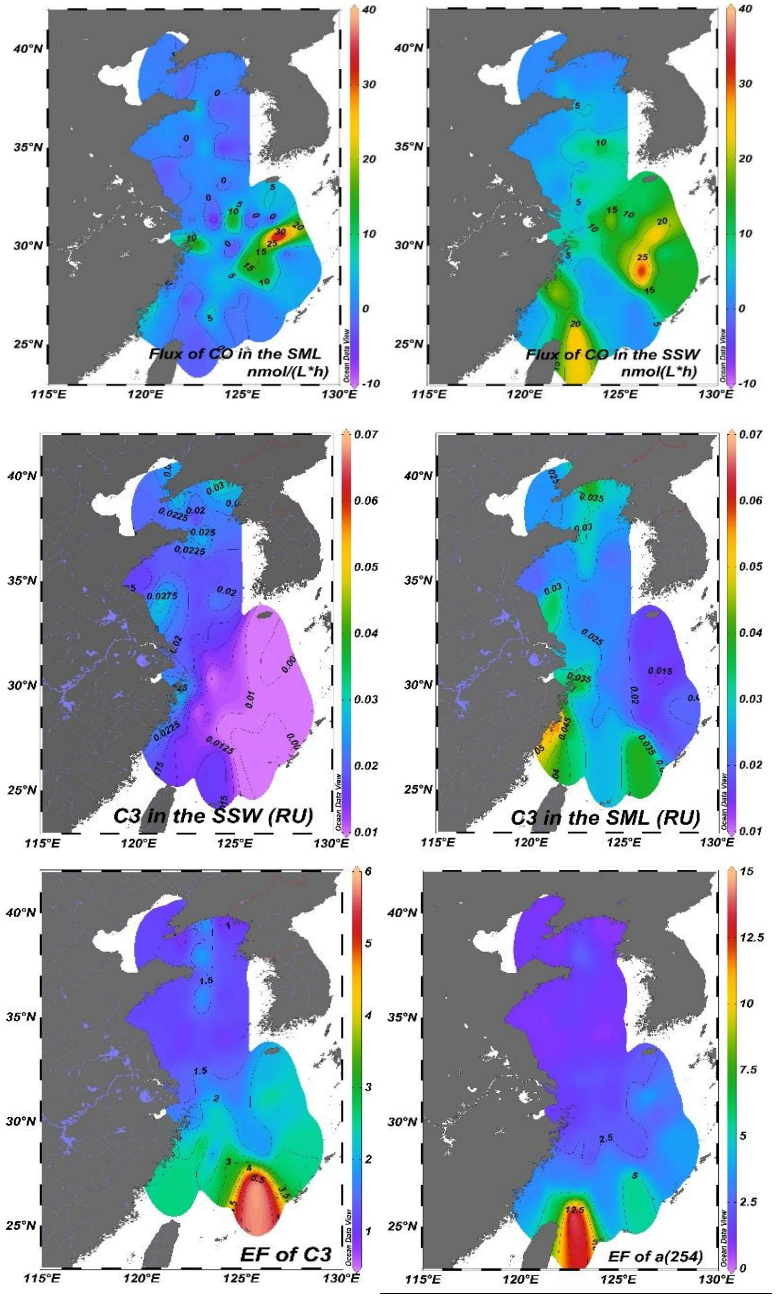

https://doi.org/10.5194/egusphere-2025-2429
Preprint. Discussion started: 5 June 2025

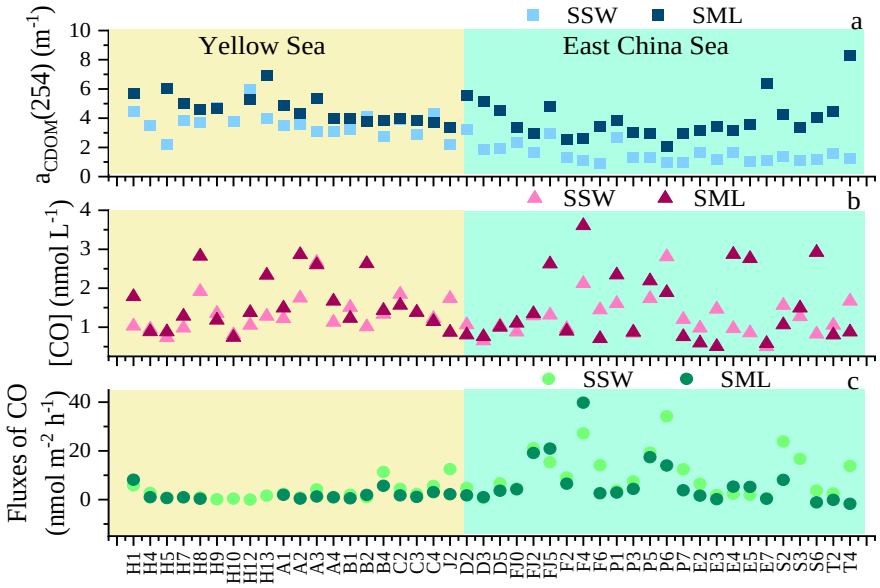

Fig. 2. Distributions of CO and the marine-like fluorescence C3 in the SSW and the SML; CO in the atmosphere, and the flux of CO in the SSW and the SML; and the enrichment factors of CO and the marine-like fluorescence C3 in the SML, and temperature and salinity in the in the East China Sea and the Yellow Sea during winter. The concentration profiles of CO in the SSW (d) resemble those of CO in the SML, which is evidence for biogeochemically very stable, salt-like (conservative) properties.

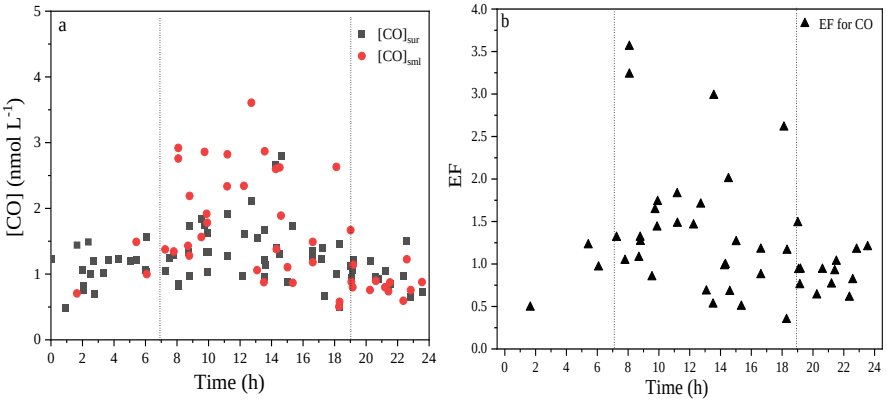

https://doi.org/10.5194/egusphere-2025-2429
Preprint. Discussion started: 5 June 2025

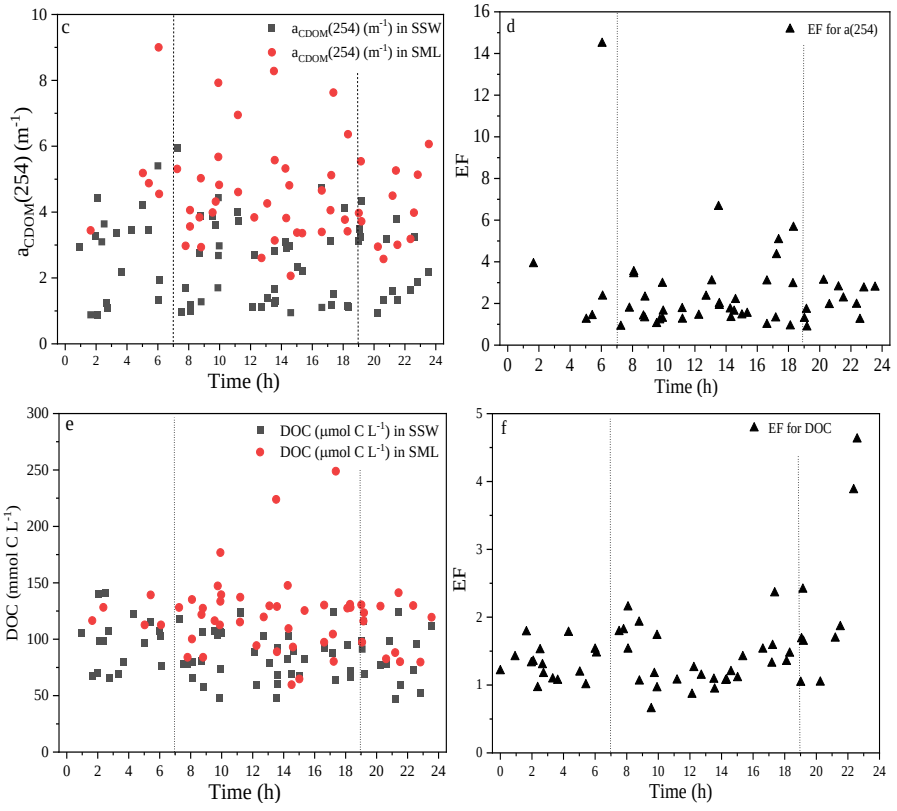

Fig. 3. Variations in the $[CO]_{sml}$, $[CO]_{ssw}$, $a_{CDOM}(254)$, and DOC, EFs of [CO], $a_{CDOM}(254)$, and DOC with the sampling time at each station.

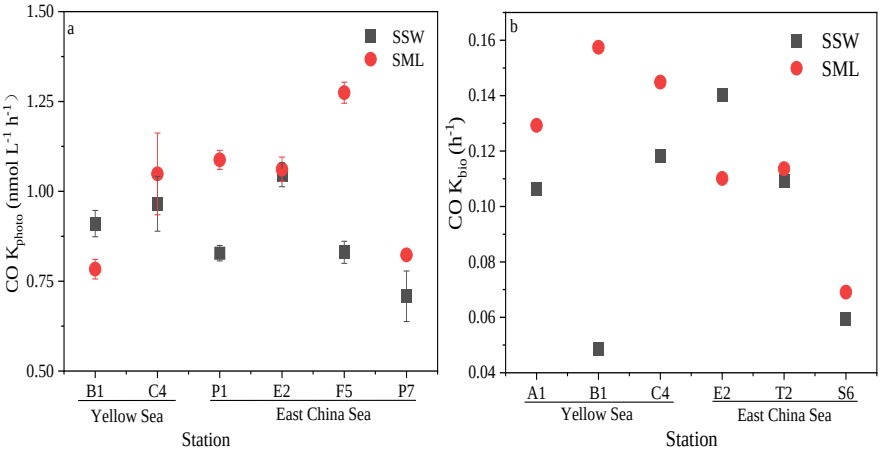

Fig. 4. Variations in photochemical CO production rate of CO (K_{photo}) in the SML (red) and the SSW (black) (a)). Variations in microbial consumption rate constants of CO (K_{bio}) in the SML

https://doi.org/10.5194/egusphere-2025-2429
Preprint. Discussion started: 5 June 2025

(red) and the SSW (black).

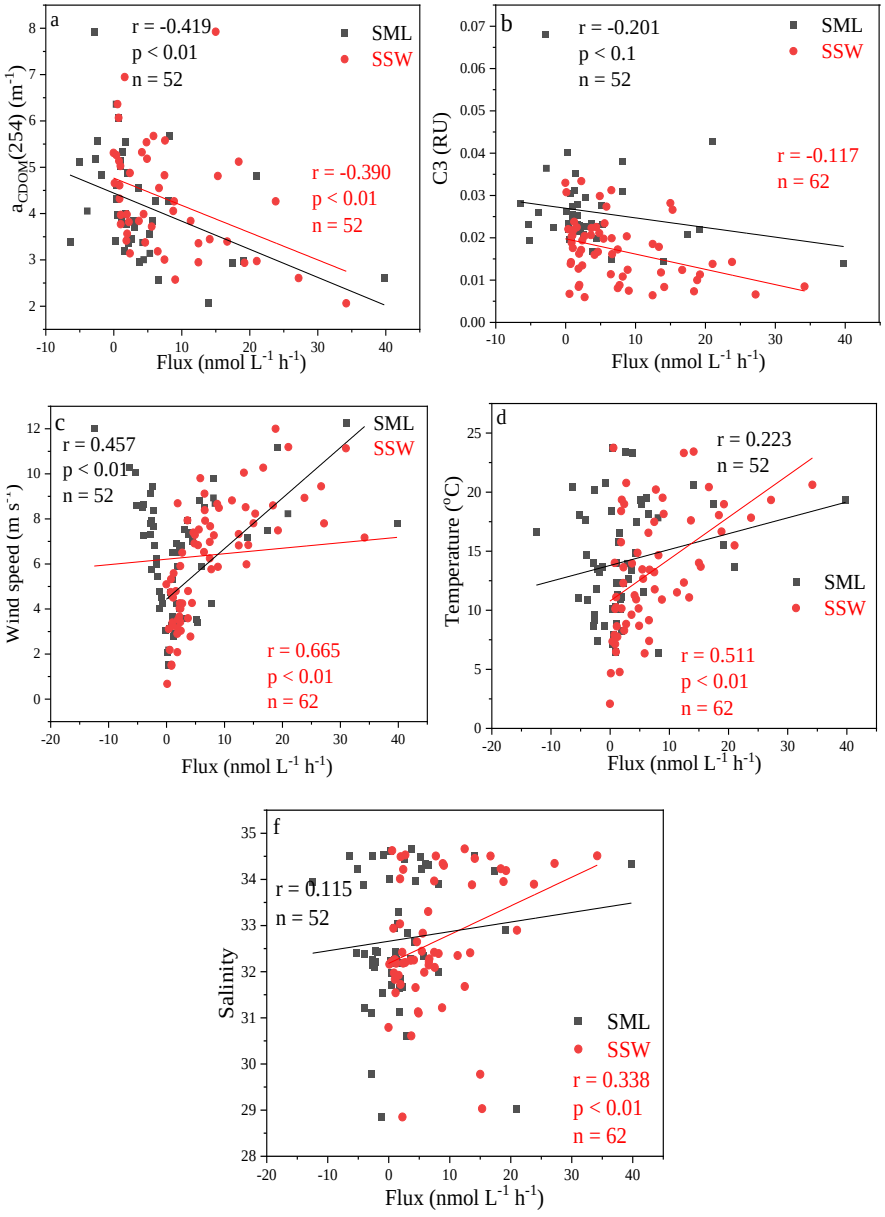

Fig. 5. Correlations between the instantaneous sea-to-air fluxes of CO (Flux) in the SSW and the SML with $a_{CDOM}(254)$, marine humic-like C3, wind speeds, temperature, and salinity in the East China Sea and the Yellow Sea during winter.

https://doi.org/10.5194/egusphere-2025-2429
Preprint. Discussion started: 5 June 2025

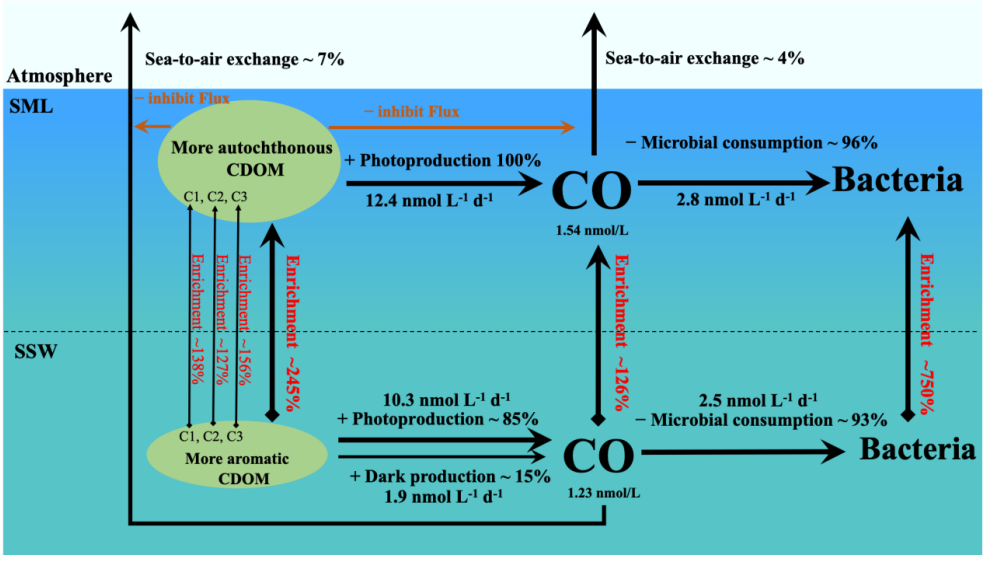

Fig. 6. Budget model of CO transformation in the SML and the SSW in the eastern marginal seas of China during winter. (Bacterial enrichment was calculated by Sun et al., 2020).

https://doi.org/10.5194/egusphere-2025-2429
Preprint. Discussion started: 5 June 2025

Table 1 Correlation coefficients between [CO], CDOM optical parameters, DOC, Chl-*a*, O_2, salinity, and temperature in SSW a) and SML b).

a)

	$[CO]_{ssw}$	Temperature	Salinity	O_2	$a_{CDOM}(254)$	$a_{CDOM}(330)$	$a_{CDOM}(355)$	C1	C2	C3	DOC	Chl-*a*	$SUVA_{254}$	$S_{275-295}$	$S_{350-400}$
Temperature	-0.001														
Salinity	0.017	0.699**													
O_2	-0.072	-0.977**	-0.723**												
$a_{CDOM}(254)$	-0.029	-0.907**	**-0.716****	0.876**											
$a_{CDOM}(330)$	-0.118	-0.783**	**-0.690****	0.758**	0.939**										
$a_{CDOM}(355)$	-0.151	-0.717**	**-0.622****	0.690**	0.894**	0.990**									
C1	0.008	-0.591**	**-0.758****	0.596**	**0.675****	0.680**	0.632**								
C2	0.053	-0.324*	**-0.341****	0.286*	**0.533****	0.592**	0.599**	0.759**							
C3	-0.049	-0.788**	**-0.851****	0.779**	**0.894****	0.887**	0.838**	0.891**	0.665**						
DOC	0.008	-0.598**	-0.239	0.583**	**0.532****	0.394**	0.354**	0.241	0.146	0.323*					
Chl-*a*	0.109	-0.357**	-0.092	0.415**	**0.333****	0.235	0.208	0.104	0.159	0.215	0.348**				
$SUVA_{254}$	-0.081	-0.676**	-0.705**	0.654**	**0.824****	**0.860****	**0.831****	**0.653****	**0.560****	**0.853****	-0.006	0.134			
$S_{275-295}$	0.045	0.100	0.099	-0.092	-0.204	-0.385**	-0.448**	-0.197	-0.241	-0.269*	-0.009	0.084	-0.241		
$S_{350-400}$	-0.001	0.009	-0.060	0.044	-0.095	-0.214	-0.279*	0.009	-0.103	-0.043	-0.088	0.026	-0.050	0.867**	
S_R	0.059	0.346**	0.421**	-0.429**	-0.254*	-0.220	-0.134	-0.343**	-0.104	-0.393**	-0.087	-0.148	-0.316*	-0.506**	-0.645**

*Correlation is significant at the 0.05 level (two-tailed).

**Correlation is significant at the 0.01 level (two-tailed). N = 44.

https://doi.org/10.5194/egusphere-2025-2429
Preprint. Discussion started: 5 June 2025

b)

	$[CO]_{sml}$	Temperature	Salinity	SML $a_{CDOM}(254)$	SML $a_{CDOM}(330)$	SML $a_{CDOM}(355)$	SML C1	SML C2	SML C3	SML DOC	SML $SUVA_{254}$	SML $S_{275-295}$	SML $S_{350-400}$
Temperature	-0.032												
Salinity	-0.098	0.699**											
SML $a_{CDOM}(254)$	-0.137	-0.037	-0.045										
SML $a_{CDOM}(330)$	-0.119	-0.113	-0.135	**0.948****									
SML $a_{CDOM}(355)$	-0.143	-0.114	-0.146	**0.901****	0.989**								
SML C1	-0.095	0.158	-0.156	**0.711****	0.504**	0.434**							
SML C2	-0.217	0.089	-0.106	**0.670****	0.675**	0.673**	0.702**						
SML C3	-0.060	0.092	-0.154	**0.823****	0.622**	0.541**	0.938**	0.703**					
SML DOC	-0.018	0.136	0.174	**0.898****	0.783**	0.705**	0.572**	0.280	0.665**				
SML $SUVA_{254}$	-0.063	-0.250	-0.439**	0.136	0.303*	0.376**	0.240	**0.501****	0.262	-0.272			
SML $S_{275-295}$	0.254	0.241	0.223	0.040	-0.217	-0.318*	0.323*	-0.056	0.336*	0.216	-0.409**		
SML $S_{350-400}$	0.270	0.112	0.082	0.136	-0.090	-0.187	0.385**	0.047	0.427**	0.244	-0.281	0.968**	
SML S_R	-0.288	0.231	0.213	-0.248	-0.057	0.044	-0.276	0.029	-0.339*	-0.296*	0.167	-0.726**	-0.776**

*Correlation is significant at the 0.05 level (two-tailed).

**Correlation is significant at the 0.01 level (two-tailed). N = 44.

https://doi.org/10.5194/egusphere-2025-2429
Preprint. Discussion started: 5 June 2025

Table 2 Correlation coefficients between EFs of CO, DOM absorption, DOC, three fluorescence components, temperature, salinity, and wind speed.

	EF of CO	EF of DOC	EF of $a_{CDOM}(254)$	EF of $a_{CDOM}(330)$	EF of $a_{CDOM}(355)$	EF of C1	EF of C2	EF of C3	Temperature	Salinity	Wind speed
EF of DOC	-0.098										
EF of $a_{CDOM}(254)$	-0.067	0.867**									
EF of $a_{CDOM}(330)$	-0.111	0.726**	0.912**								
EF of $a_{CDOM}(355)$	-0.124	0.556**	0.752**	0.945**							
EF of C1	0.081	0.731**	0.898**	0.753**	0.619**						
EF of C2	-0.084	0.149	0.586**	0.600**	0.580**	0.486**					
EF of C3	-0.022	0.796**	0.935**	0.830**	0.714**	0.964**	0.502**				
Temperature	0.037	**0.363****	**0.528****	**0.533****	**0.456****	**0.617****	**0.296***	**0.604****			
Salinity	0.006	**0.289***	**0.478****	**0.493****	**0.427****	**0.500****	**0.268**	**0.491****	0.699**		
Wind speed	-0.177	0.008	0.186	0.159	0.161	-0.130	-0.006	-0.105	0.129	0.052	
Solar irradiance	**0.409****	-0.024	-0.051	-0.082	-0.050	0.022	-0.139	0.002	0.160	0.157	0.104

*Correlation is significant at the 0.05 level (two-tailed).

**Correlation is significant at the 0.01 level (two-tailed). N = 44.